FINAL GALILEO PROPULSION SYSTEM IN-FLIGHT CHARACTERIZATION

T.J. Barber*
Jet Propulsion Laboratory
California Institute of Technology
Pasadena, California

F.A. Krug† and K.P. Renner†
Deutsche Forschungsanstalt für Luft- und Raumfahrt e.V. (DLR)
Oberpfaffenhofen, Germany

Abstract

The Galileo Retro-Propulsion Module (RPM) performed excellently throughout the ambitious, eight-year Galileo Jupiter mission. The RPM is a state-of-the-art, pressure-fed, bipropellant propulsion system, provided to NASA by the Federal Republic of Germany. Some Galileo RPM pressure transducers drifted linearly versus time since launch. Consumable usage was generally well within specifications, including propellant usage. Maneuver performance continued to be excellent during the orbital tour of Jupiter. No 1O-N thruster thermal instabilities were observed during the mission, likely due to a conservative, pulse-mode operating strategy. Apparent performance shifts of the lateral thrusters were detected and remain unexplained. Nearly all Galileo 1O-N thrusters exceeded ground performance thrust levels by 10/. to 5%. The soft-seat pressure regulator, now isolated, exhibited exemplary performance during the Galileo mission. Conversely, oxidizer and fuel check valve performances were out of specification and highly non-repeatable for the three main 400-N engine burns. However, the 400-N engine performances were only slightly impacted, and a highly successful Jupiter Orbit Insertion and orbital tour were realized.

L Introduction

Galileo's voyage of discovery continues to rewrite the textbooks of planetary science in the 1990's. Originally conceived more than twenty years ago, the Galileo nominal mission is nearing completion after a challenging eight years in flight. The three primary science objectives of the Galileo mission are (1) to investigate the physical state and chemical composition of the Jovian atmosphere, (2) to investigate the physical state and chemical composition of the Jovian satellites, and (3) to investigate the physical structure and dynamics of the Jovian magnetosphere.

The Galileo spacecraft, comprised of an atmospheric entry probe and orbiter, was launched October 18, 1989, aboard the space shuttle Atlantis. An Inertial Upper Stage (IUS) booster placed Galileo on the proper heliocentric path, a six-year looping Venus-Earth-Earth-Gravity Assist (VEEGA) trajectory to Jupiter (see Figure 1). This circuitous route was necessary given the many mission constraints and redesigns following the Challenger disaster in 1986.'

Galileo's VEEGA cruise was far from uneventful. Flybys of Venus and the Earth (twice) were executed successfully, both with respect to

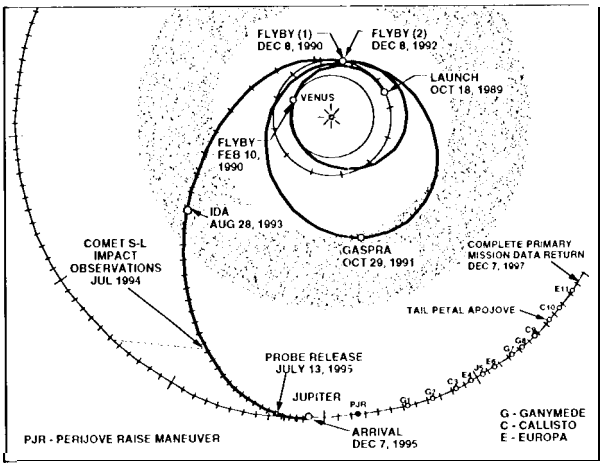

Figure 1: Galileo Heliocentric Trajectory

* Member Technical Staff
† Wissenschaftlicher Mitarbeiter der DLR

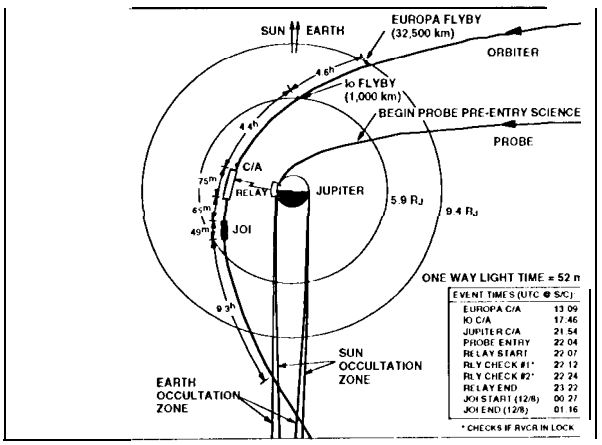

Figure 2: Galileo Jupiter Arrival Geometry

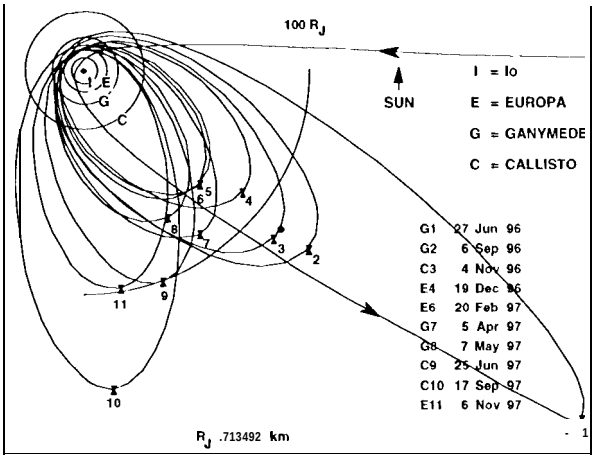

Figure 3: Galileo Jovian Orbital Tour Petal Plot

unique science observations and with respect to the acquisition of the proper gravity assists to get to Jupiter. First-rate planetary science was accomplished during VEEGA as well, including (1) the first reconnaissance of a main-belt asteroid, 951 -Gaspra, October, 1991; (2) the first discovery of a natural satellite (Dactyl) of an asteroid, 243-Ida, August, 1993; and (3) the first and only telescope to directly image a comet or asteroid (fragments of Comet Shoemaker-Levy 9) impacting a planet (Jupiter).

Along with profound science successes, there were many notable engineering successes during VEEGA. The Jupiter atmospheric entry probe was successfully released on July 13, 1995. Two weeks later, the Galileo 400-N (main) engine was used post-launch for the first time, with great success. Prior to 1995, the main engine was last fired in June, 1983. Perhaps most stunningly, on December 7, 1995 (PST), Galileo recorded a unique success in the history of planetary exploration—the first entry into an outer (giant) planet atmosphere (by the probe) and the first orbital capture around a giant planet (by the orbiter). Figure 2 displays the Galileo arrival geometry, demonstrating the time criticality of these two mission-essential events.

Coupled with the successes, however, were some noteworthy engineering setbacks during VEEGA. A partially deployed (and hence unusable) High Gain Antenna (HGA) and a "sticky" Data Memory Subsystem (DMS) tape recorder brought special challenges to the Galileo flight team. Fortunately, the flight team was able to overcome these challenges through modifications to the ground receivers of the Deep Space Network (DSN), extensive changes to Galileo flight software, an improved DMS tape conditioning profile, and additional new DMS-related autonomous fault protection routines.

After orbit insertion, the orbiter began touring Jupiter's "miniature solar system," executing multiple orbits about Jupiter (see Figure 3), all but one with a very close satellite flyby (of Europa, Ganymede, or Callisto). These close encounters with the satellites not only allow detailed scientific investigation, the gravity assist obtained from the target satellite literally enables the orbital tour.'

The nominal Galileo End-Of-Mission (EOM) is December, 1997. A follow-on mission utilizing the Galileo orbiter—the Galileo Europa Mission (GEM)—was recently approved. This two-year mission, from December, 1997 to December, 1999, will continue to unveil the mysteries of the Jovian system, with repeated Europa flybys followed by four repeated Callisto encounters and one nominally planned close encounter with volcanically active 10.

il. **The Spacecraft**

Galileo was the second planetary spacecraft to be launched from the space shuttle, following the Magellan mission to Venus, which was launched May, 1989. Due to the payload bay size constraints for the shuttle, several key portions of the Galileo spacecraft were designed to be deployed following separation from the payload bay, including the HGA, Radioisotope

Thermoelectric Generator (RTG) booms, and magnetometer boom. Therefore, the launch configuration differs somewhat from the cruise configuration.

Figure 4 shows the Galileo spacecraft cruise configuration with a partially deployed HGA and the probe attached. The HGA unfurled only partially after the initial deploy command issued April, 1991, leading to an asymmetric, "claw-shaped" HGA. In 1992, the decision was made to use the LGA in case all efforts to free the bound ribs of the HGA would be unsuccessful. Several subsequent attempts to open the HGA were made, to no avail.

Unique among planetary missions, Galileo is a spin-stabilized, dual-spin spacecraft. Except for one optical instrument, the spinning (spun) portion of the spacecraft contains all the fields and particles science instruments, allowing these instruments an omni-directional view. The stationary (despun) portion of the spacecraft contains a scan platform with imaging science instruments that require stable pointing. This design, though challenging to the designers, combines both the science advantages of Voyager (three-axis stabilized) and Pioneer (spin-stabilized) in one spacecraft. A complete description of the Galileo spacecraft may be found in the literature.'

Due to the weak solar intensity at Jupiter (< 55 W/m' on average), the orbiter is powered by two RTGs. The total RTG power output decreases from 572 W at the beginning of the mission to 456 W by end-of-year 1999, the nominal completion of GEM.

The Command and Data Subsystem (CDS), with components both on the spun and despun portions of the orbiter, represents a significant improvement over the Voyager computer hardware. Closely tied to the CDS is the previously mentioned DMS, which allows spacecraft science and engineering data to be recorded and returned to Earth at a later time. The DMS is an essential mission element with a LGA-only mission—it has been used extensively to return the probe entry data as well as data from each satellite encounter during the orbital tour.

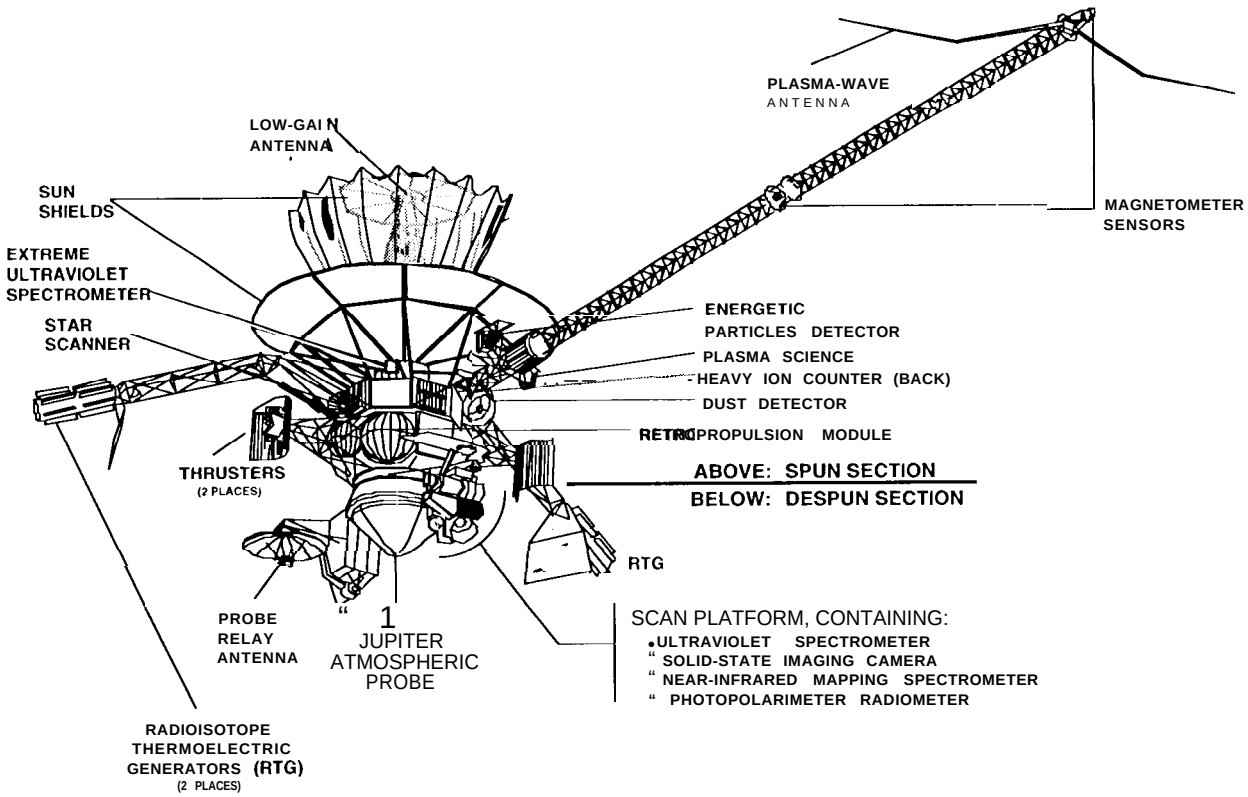

Figure 4: Galileo Spacecraft in Nominal Cruise Configuration

The telecommunications subsystem utilizes S-band uplink and downlink, primarily communicating with NASA's DSN 70-m antennas in Goldstone, California; Madrid, Spain; and Canberra, Australia. In fact, improvements in receiver hardware and signal coding (coupled with extensive Galileo flight software changes) have literally enabled the LGA-only orbital mission. No X-band command and telemetry communications have been possible, due to the HGA anomaly. The X-band radio frequency was used during HGA troubleshooting activities, however.

The Attitude and Articulation Control Subsystem (AACS) is responsible for maintaining the inertial pointing and spin rate for the Galileo spacecraft, as well as scan platform pointing. AACS attitude changes are accomplished by firing two of the twelve 10-N bipropellant thrusters of the RPM. Hence, the RPM and AACS subsystems are closely related and the RPM/AACS interface is quite critical.

Extensive on-board fault protection against a multitude of fault conditions is provided on Galileo. These fault protection algorithms are necessarily autonomous, due to long (up to almost one hour) one-way communication times, the high demand for DSN tracking coverage, and the loss of communication experienced during solar conjunction.

III. RPM Hardware Summary

The Galileo RPM is a bipropellant, pressure-fed propulsion system provided to NASA by the Federal Republic of Germany. The RPM provides all the propulsive capability necessary for the complex Galileo mission. A hyperbolic combination of monomethylhydrazine (MMH) and nitrogen tetroxide (NTO) is utilized for twelve trajectory correction and attitude (spin and pointing) maintenance 1O-N thrusters and one 400-N main engine used for large Galileo trajectory maneuvers. As shown in Figure 5, a set of six 10-N thrusters is mounted in each of two thruster clusters, which extend approximately two meters from the RPM body center on opposite booms. The 400-N engine is centered in the RPM structure and is initially covered by the probe (see Figure 4)—protected from micrometeorites by the surrounding spacecraft/probe hardware. Therefore, the engine could not be fired until the probe was released.

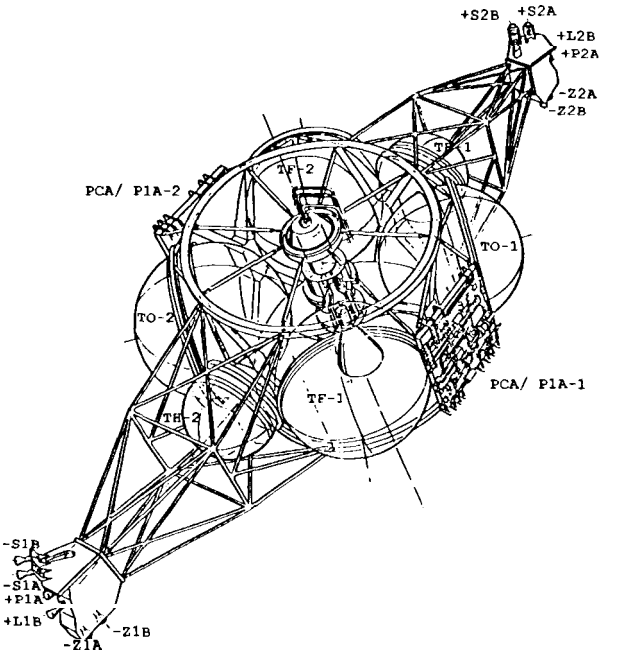

Figure 5: RPM 3D View

The RPM is a self-contained, primary load-bearing structure of the Galileo spacecraft. Principal components of the central RPM body include two helium pressurant tanks, two MMH propellant tanks, and two NTO propellant tanks, all connected with an integrating truss. Other RPM components include a pressurization and feed system, consisting of two Pressurant Control Assemblies (PCAs) on two separate equipment panels. One of these panels also carries the oxidizer feed system, called the Propellant Isolation Assembly (PIA-1), and the second includes the fuel feed system, called PIA-2. Also included is a thermal control system (for booms, thruster clusters, and the 400-N engine) consisting of thermal blankets, Radioisotope Heater Units (RHUs), electrical heaters, and electrical cabling. Details on the mission requirements, design, and pre-launch performance qualification of the RPM have been published.'

Figure 6 is the RPM pressurization and feed system schematic. A great deal of redundancy was built into the pressurization and feed system, both for shuttle safety reasons and for fault tolerance during this lengthy mission. Helium is provided to the propellant tanks via one of two redundant pressure regulators. Only the primary pressure regulator was utilized in flight.

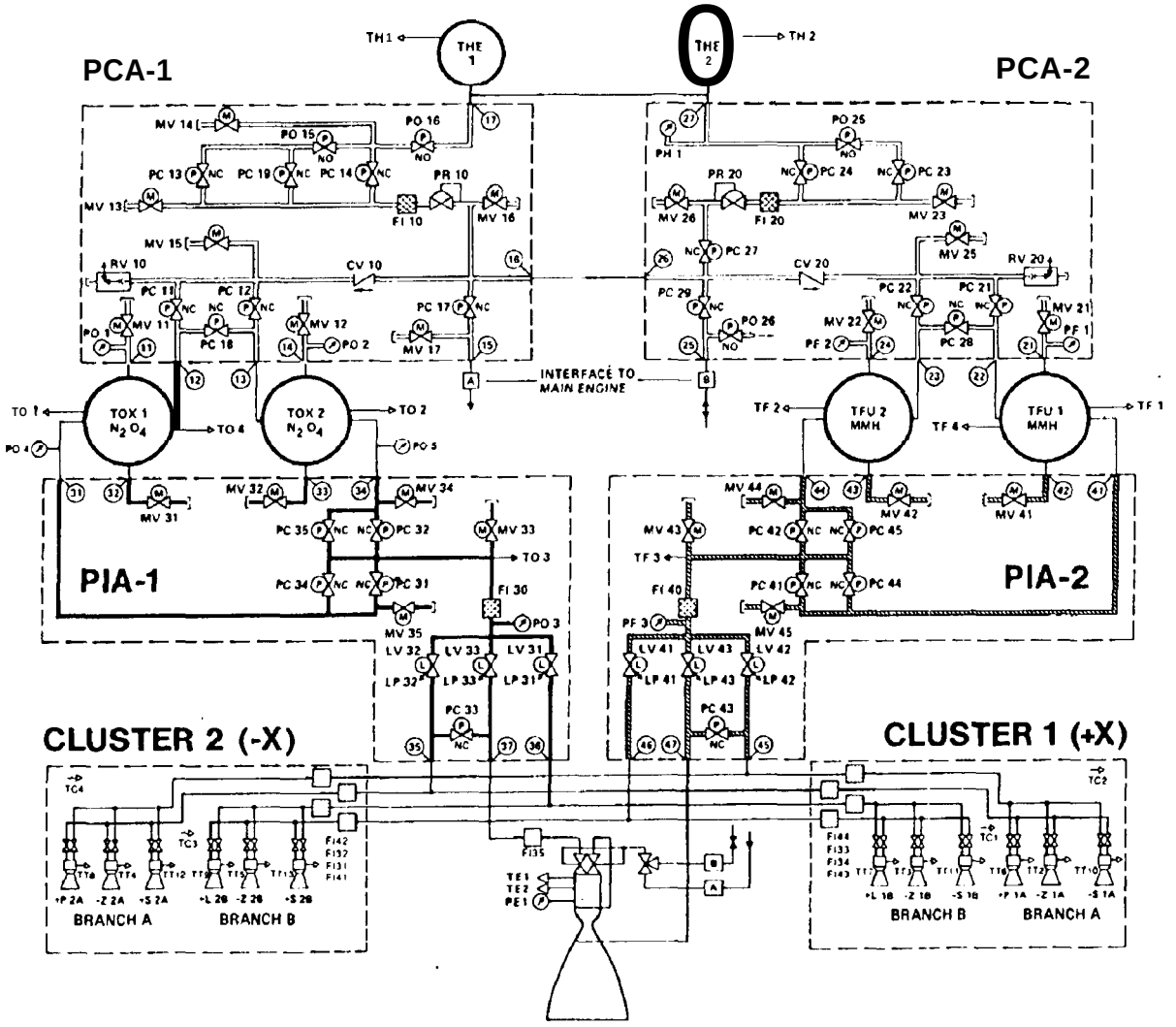

Figure 6: RPM Pressurization and Feed System Schematic

The pressurization system was designed to avoid a repetition of the regulator leakage seen on the Viking mission to Mars. A soft-seat regulator was selected to minimize sensitivity to particulate contamination. The parallel redundant regulator configuration included a backup regulator positively isolated from downstream contamination by a normally closed pyro valve. Check valves were provided to minimize MMH and NTO vapor migration upstream of the propellant tanks. Since propellant vapor mixing (after permeation through check valves) was the probable cause of the Viking regulator leak, the Galileo check valves were constructed of a unique soft-seat design that yields extremely low reverse leakage levels. To guard against possible leaking thruster valves, back-pressure relieving latch valves were provided upstream of the thrusters for reversible isolation.

The design and performance of the 10-N thruster and the 400-N engine mentioned above have been documented.' Thermal control for the 10-N thruster is accomplished by film-cooling of the combustion chamber, MMH regenerative cooling of the engine throat, and radiative cooling of the nozzle. Re-testing of the 10-N thruster in early 1989 demonstrated some thermal instabilities during continuous-mode operation and some hot operation during pulse-mode operation at certain duty cycles (duty cycle = $T_{on}/[T_{on}+T_{off}]$).[5] High oxidizer-to-fuel mixture ratios and/or high total propellant mass flow rates or higher propellant temperatures generally aggravated the instabilities and hot operation. Therefore, to preclude these

instabilities, the Galilleo RPM operates the 10-N thruster in pulse-mode only, with quite low duty cycles and with a curtailed tank pressure and temperature range. This mode of operation, though challenging to the flight team, has worked well in flight, as is evident from the excellent Galileo navigation throughout the mission.

Thruster thermal performance is determined from temperature transducers mounted to the cluster and thruster chambers. Four of the 10-N thruster temperature transducers failed early in the mission.[6] This has little consequence for the mission since cluster temperatures adequately characterize 10-N thruster thermal performance.

IV. Galileo 1O-N Thruster Operation

The ambitious nature of the Galileo mission puts severe demands on the propulsion system for attitude maintenance, Trajectory Correction Maneuvers (TCMs) during cruise, Orbit Trim Maneuvers (OTMs) during orbital tour, and large Av maneuvers—specifically, the Orbiter Deflection Maneuver (ODM), Jupiter Orbit insertion (JOI) burn, and the PeriJove Raise (PJR) maneuver. Many attitude correction functions are provided for the dual spinning Galileo. First, spin corrections to the nominal (all-spin or dual-spin) spin rate are allowed for, correcting solar torques and maneuver errors caused by thruster misalignments, engine performance changes, etc. In addition, large spin-rate change maneuvers (from 2.89 rpm to 10.5 rpm in all-spin mode) are a mission requirement for probe attitude stabilization, prior to probe release, since the Jovian atmospheric entry probe has no attitude correction capability. Also, operation of the 400-N engine requires a minimum spin rate near 10 rpm as well, for centrifugal propellant management in the propellant tanks during the 400-N acceleration, as well as for thrust vector control. Two sets of redundant spin-up and spin-down thrusters are used for these purposes (see Figure 7). Nominally, the S2A and S1 A thrusters are the primary spin-up and spin-down thrusters, respectively.

The capability to turn the spacecraft by means of a precession maneuver is necessary in the Galileo mission for thermal reasons (early mission only), acquiring science data, maintaining communication with the Earth and maintaining celestial reference, and finally for so-called turn-burn maneuvers. Three types of precession

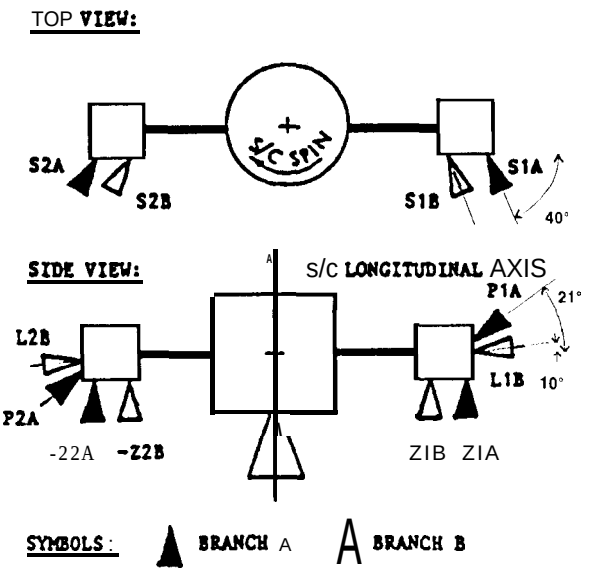

Maneuver	Operated Thruster Branch A	Branch B
Attitude Control:		
- Spin-Up	S2A	S2B
- Spin-Down	SIA	S1 B
- Precession Control	P1A/P2A	L1 B/L2B
- Turns	Z1A/Z2A	Z1B/Z2B
Trajectory Control:		
- Plus-Axial Av	PIA	LIB
- Minus-Axial Av	Z1A/Z2A	Z1B/Z2B
- Lateral Av	P1A/P2A	L1 B/L2B

Figure 7: RPM IO-N Thruster Configuration

maneuvers have been executed—Spacecraft Inertial TURNS (SITURNS), sun acquisitions, and HGA (pointing) corrections. SITURNS may be performed in two different modes—balanced or unbalanced. Balanced SITURNS are performed on the P-thrusters, firing simultaneously once per spacecraft revolution to cancel out the net Av, as may be seen in Figure 7. Conversely, unbalanced SITURNS may be executed by firing either the A-branch or B-branch Z-thrusters alternately, once per revolution. Note that in this case, a deterministic Av is imparted to the spacecraft. Unbalanced turns are nearly three times more propellant-efficient than balanced turns, but the associated Av must be accounted for in trajectory optimization. Both types of turns have been utilized extensively during the Galileo mission.

HGA (or pointing) corrections allow the HGA boresight as well as the LGA boresight to be

pointed to the Earth. Though the spacecraft exclusively uses a wider beam S-band telecommunication link over LGA-1 (which has the same boresight direction as the HGA), LGA-1 pointing tolerances are also quite tight due to the aggressive data return strategy from the Jupiter system (given the HGA deployment failure). In addition, pointing corrections are necessary during maneuvers because thruster misalignments or performance shifts can cause the spacecraft to precess sufficiently such that the AACS star set chosen for the maneuver (for accurate attitude reference) is no longer viable. Like balanced SITURNS, pointing corrections are performed on the P-thrusters in a balanced mode.

Sun acquisitions allow the spacecraft to start at any off-sun attitude and return to (near) sun-point. They are performed also using the P-thruster couple, but since their on-times are not individually calculated to balance their impulse, a small Av is imparted to the spacecraft during a sun acquisition. These maneuvers were used sparingly in the last few years, since celestial reference was almost always available (and hence the use of SITURNS was possible).

Many relatively small TCMS and OTMS (Av < 40 m/s) are necessary throughout interplanetary cruise and the Jovian orbital tour. These maneuvers are basically of two types—deterministic and statistical. The capability to perform these relatively small maneuvers is provided in both the *z-direction (along the spacecraft spin axis) and in the lateral direction. A "vector mode" maneuver represents one way, then, to perform a given maneuver. In this case, the spacecraft's attitude remains unchanged throughout the maneuver and the proper amount of Av is achieved by splitting the Av into the correct amount of lateral and (±) axial firing. Alternatively, the maneuver may be accomplished by first processing to the appropriate attitude ("turn"), firing along either the lateral or axial direction ("burn"), and then processing back ("unwind") to the original attitude via a SITURN or sun acquisition. Such turn-burn-unwind maneuvers can offer propellant savings when compared with the analogous vector mode maneuver, depending on Av magnitude and direction.

Lateral thruster segments have been employed very frequently in Galileo TCMS and OTMS. In this operating mode, the L1 B and L2B thrusters fire alternately, once per revolution. The thruster on-times are set individually such that the net torque on the spacecraft is zero. However, a small Av component is generated along the z-axis each time a lateral maneuver is executed which is accounted for in the maneuver design. Since the inertial firing position (clock angle) may be specified for a lateral maneuver, a lateral Av may be achieved in any lateral direction.

Two types of 10-N thruster axial maneuvers have been executed on Galileo. The most common is a PULZ (axial -z) maneuver, which imparts a velocity increment to the spacecraft in the -z direction. Unlike the unbalanced turn mode, this type of maneuver fires each of two Z-thrusters simultaneously twice per revolution, canceling the net torque. Another type of axial maneuver is the POSZ (axial +z) maneuver, which increases the spacecraft velocity in the +z direction. As may be seen in Figure 7, only the PIA and LIB thrusters have a thrust component in the spacecraft +z direction. A POSZ maneuver does not cause the spacecraft to precess, since the PI A thruster is fired twice per revolution, applying opposite torques. Since the thrust component of PIA thruster in the +z direction is not large (sin 210), this type of maneuver is not very efficient and is generally avoided, if possible, even by occasionally biasing the trajectory slightly.

There is one common Galileo propulsive activity that is performed to maintain the RPM. At least every twenty-three days (a number determined through theoretical modeling), all RPM 1O-N thrusters are operated for a minimum on-time of 1.2 s. These so-called thruster '(flushes" are necessary to limit the build-up of products from the interaction of NTO with some small stainless steel components (nearly all hardware in contact with NTO is made of a titanium alloy which resists such corrosion). These products may accumulate to the point that they could clog filters or small flow passages.' There has been no evidence of such contamination during the Galileo mission.

Flushing maneuvers are designed to impart as little Av as possible, but it is clear that the Av in the -z direction (from all the Z-thrusters) will not cancel. Navigation has accepted this Av in the -z direction, since it is of small magnitude (< 35 mm/s for all four Z-thrusters, total) and, more importantly, because it is predictable in magnitude and direction. These thruster flushes have had little

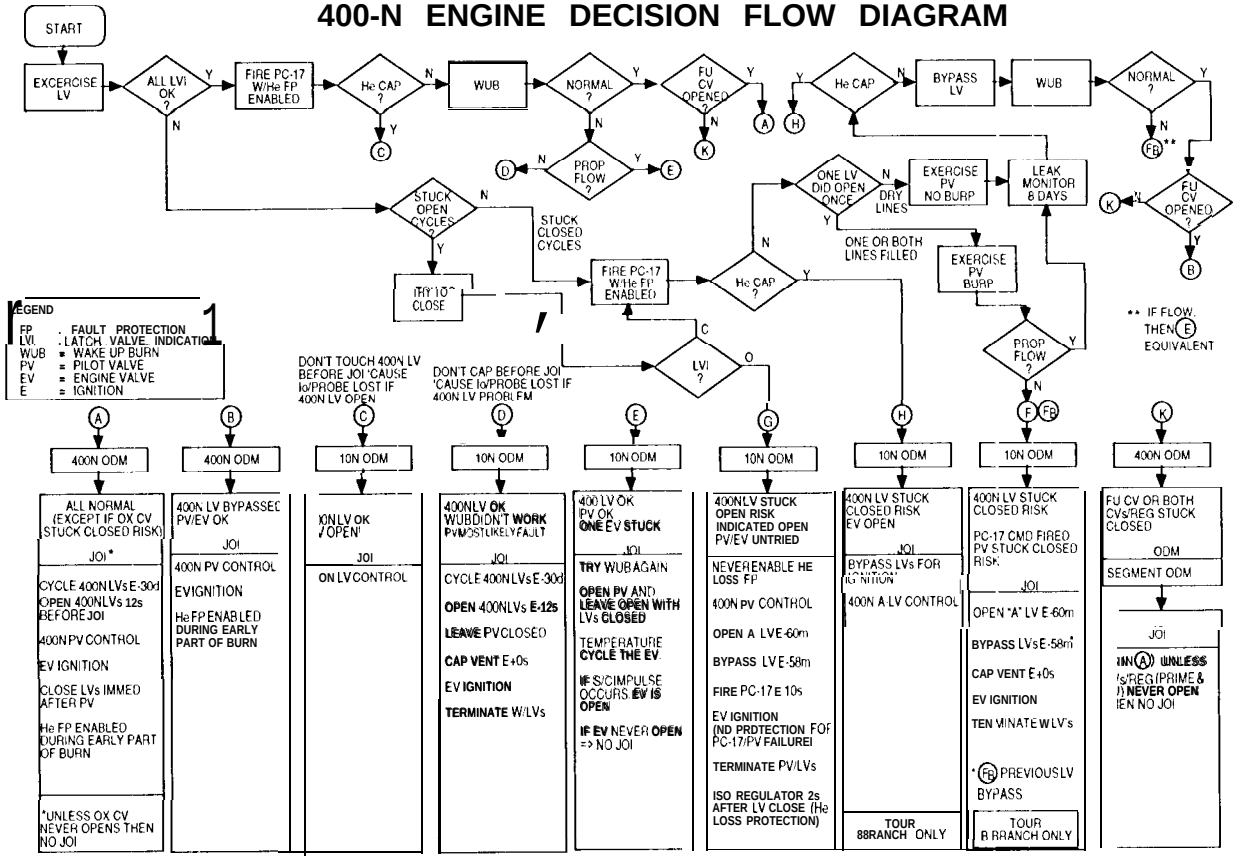

Figure 8: 400-N Engine Flow Diagram

operational impact on the Galileo mission, since trajectory correction has not been adversely affected and because the total propellant cost of thruster flushes throughout the entire mission is only around 8.5 kg (<1?'. of the total usable propellant). One side benefit of the thruster flushes is the ability to analyze 10-N thruster performance versus ground test performance for otherwise unused engines like the B-branch S-thrusters.

V. 400-N Enaine Operation

Operation of the Galileo 400-N engine brought very different challenges to the propulsion system given the six year "in-flight" wait time before its first use. The correct operation of all hardware components was partially verified, components which include latch valves, pneumatically controlled engine valves, an electromagnetic pilot valve, propellant filters, oxidizer and fuel check valves and the pressure regulator. Figure 8 represents the flow diagram that was developed to accomplish these checks. In order to minimize the adverse effect of a valve failure (stuck open or stuck closed), two diagnostic activities were performed in-flight prior to the first nominal burn. Before pressurization of the pilot valve, the 400-N latch valves were commanded (opened/closed) 25 times. All actuations were successful as indicated by reed switches. The function of the pilot valve is to pneumatically actuate the engine valves, which starts a 400-N engine burn. A two-second (wake-up) burn was performed to verify the engine valves and pilot valve open/close functions and also to positively confirm the open state of the latch valves during the burn. The wake-up burn did verify that the engine and all associated valves worked properly.

All 400-N burns are accelerometer controlled, unlike 10-N thruster firings. The required Av is commanded to the spacecraft and the on-board burn task compares this value with the one which is derived from the accelerometer. As soon as the commanded Av is achieved, the burn is shut down.

Because the accelerometer mainly contributes to the Av uncertainty, a calibration burn would be valuable to assure a high accuracy at the critical Jupiter Orbit Insertion. Therefore, the less time critical ODM, performed on the 400-N engine, served also as an accelerometer calibration burn.

A major effort during the preparation of the 400-N burns was put into the development of new/updated autonomous on-board fault protection routines to avoid mission critical impacts from malfunctioning propulsion system hardware during a burn. Potential internal helium leaks in the pilot valve were guarded against by monitoring the helium tank pressure; they could have been mitigated by firing a pyre-valve and thus closing the open pilot valve port ("helium-loss" protection). This would have required subsequent engine operation control via the latch valves only, an operational mode which was tested during ground tests in Germany in 1994 and 1995. The "over-pressure" algorithm checked the propellant tank pressures against an upper limit. It would have isolated the pressure regulator if the tank pressures were to rise above a set limit. A "low-pressure" protection was implemented to shut down the engine in case the propellant line pressures dropped below a specified limit, possibly caused by plugged filters. Nominal changes in tank pressures required the maintenance of the thresholds, especially for the "helium-loss" protection. Risk assessments, fault probabilities and the criticality of a given maneuver for the mission led to the decision that "helium-loss" protection was to be used for all three 400-N maneuvers, the "over-pressure" protection for ODM and PJR and the "low-pressure" protection for PJR only.

An algorithm to protect against accelerometer malfunction was active during 400-N burns. Undetectable sensor errors would shift the burn time to the highest or lowest value. To protect against large accelerometer errors, the burn time was forced to stay between a minimum and a maximum limit. In case a total accelerometer failure would have been detected, the burn time would have defaulted to a nominal value. These parameters were set for each burn according to the expected system performance and the criticality of the maneuver.

The PJR Maneuver completed the 400-N operations. Now only one requirement remains: the engine temperature has to stay warm enough to keep the propellant in the wetted lines, valves and volumes from freezing. This requirement is accomplished by a prime and redundant heater. The remainder of mission will be performed on 10-N thrusters in blow-down mode—the regulator was isolated post-PJR.

VI. Consumable Summary

The primary RPM consumables are propellant (MMH and NTO) and latch and engine valve cycles (for both the IO-N thrusters and the 400-N engine). The usable propellant remaining is one of the most critical spacecraft consumables since it may be a life-limiting resource for the GEM mission. However, accumulated radiation damage and, less likely, RTG power output decay are contenders as well. Also, given additional usage of the 1O-N thrusters during GEM, 1O-N latch and thruster valve cycles are important consumables as well.

10-N thruster and 400-N engine models have been developed based on ground test data. From these models, estimates of the oxidizer and fuel consumption during a given maneuver may be obtained. Specifically, the oxidizer and fuel tank pressures, maneuver on-time, and propellant temperatures are entered as input. Output from the model includes the specific impulse (Isp), total mass flow, engine thrust, and mixture ratio. From the total mass flow and mixture ratio, the oxidizer and fuel consumed during the maneuver can be determined.

Despite a large unexpected propellant expenditure (approximately 50 kg) for HGA deployment attempts, the propellant margin (i.e., propellant left at the end of mission) has improved substantially since launch. In particular, the usable propellant remaining at the end of the nominal tour (at a 90% confidence level) has increased from -58 kg at launch to a current value of +49 kg. Positive propellant margins exist even at the end of GEM, with values of +19 kg following the first 10 flyby in late 1999 and +9 kg after a subsequent 10 flyby (and end of GEM). This marked improvement in propellant margin is primarily due to improvements in optimization of the placement and magnitude of TCMS and OTMS, excellent navigation, the selection of a very low Av cost orbital tour, and the use of unbalanced turns versus more costly balanced turns.

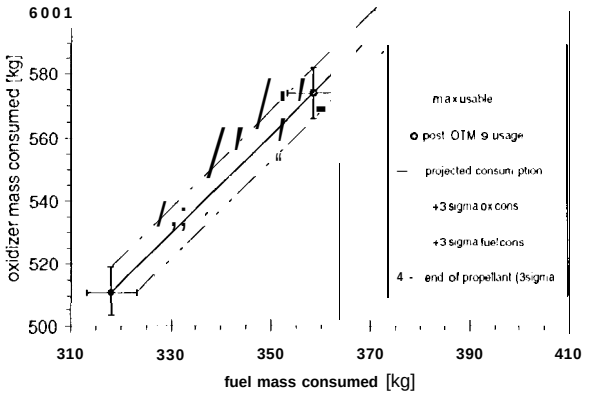

Figure 9: Usable Propellant Masses and Residuals

It is clear that in a bipropellant system like Galileo, the usable propellant is a strong function of the actual mixture ratio used by the propulsion system. Post-launch test data indicates the 10-N mixture ratios as modeled by the RPM Analysis Team may have a 4% overprediction.[8,9] A more recent analysis taking into account the actual usage of the thrusters adjusts this number to 2%. Also, pressure transducer drift uncertainties elucidated in Chapter X also cloud the determination of the actual mixture ratio used. In fact, the latter effect applies to all mission propellant, not just the 30% or so expelled through the 10-N thrusters.

Each maneuver has been carefully reconstructed using the observed telemetry for the propellant tank pressures and propellant temperatures. Figure 9 shows the calculated oxidizer and fuel consumption (as of 15-Mar-97) with their uncertainties shown by the error bars ("cross") in the lower left corner. The cross on the upper right shows the propellant masses when the fuel is depleted (in a 3σ case) assuming a mixture ratio of 1.555 for the remainder of the mission. A total of 27 kg of propellant have to be set aside to cover the past and future consumption uncertainties, the "remaining", the propellant loading uncertainties, as well as the real propellant holdup in the propellant lines and tanks. A pre-launch estimate had 34 kg of propellant labeled as "unusable." Now 7 kg of that have been released as usable. This increase is also reflected in the propellant margin numbers given above and illustrates how reserve for uncertainties can be released as more information is gathered.

Table 1 shows a summary of the propellant usage during the Galileo mission through March 15, 1997. Notice that the vast majority of usable propellant was used during 400-N engine and 10-N ΔV thruster maneuvers. Two-thirds of the total propellant usage occurred during the three large 400-N engine burns: ODM, JOI, and PJR. It is noteworthy that more propellant was used to try to deploy the HGA than was used for nominal attitude control throughout the entire mission (to date). Science turn usage is well within allocations; these maneuvers turn the spacecraft for science observation purposes only. Incidentally, if the propellant were used to depletion (not likely, given the propellant margin numbers mentioned above), the most likely outcome would be that the MMH supply would deplete first, with approximately 13.7 kg of NTO remaining unused in the Ox tanks.

Table 1: Propellant Usage Breakdown

As of March 15, 1997	Ox [kg]	Fu [kg]	Total [kg]
RPM Maintenance	4.18	2.72	6.90
Attitude Control	20.87	13.46	34.33
HGA Anomaly Activity	30.51	19.96	50.46
Science Turns	1.92	1.22	3.14
Delta-V Maneuver			
400N	377.60	228.70	606.31
10N	90.83	59.69	150.53
Total consumed	525.92	325.75	851.67
Real Holdup	2.25	0.60	2.85
Consumption Uncertainty (3σ	7.87	5.16	13.03
Remaining at 3σ Fu Depletior	10.98	0.00	10.98
Still Usable	47.78	32.69	80.47
Total Loaded	594.80	364.20	959.00

The RPM Analysis Team is also the cognizant group for latch and thruster valve cycles. Latch valves are actuated once for each separate propulsive event, such as a maneuver segment (10-N or 400-N), SITURN, spin or HGA correct, etc. The limit on latch valve cycles is 4000 per each of the 10-N A- and B-thruster branches, as well as the 400-N engine branch. As of March 15, 1997, there were 1115 cycles (27.9% of lifetime) on the 10-N A-branch oxidizer and fuel latch valves, 625 (15.6% of lifetime) on the 10-N B-branch latch valves, and 30 (0.8% of lifetime) on the 400-N latch valves. Latch valve cycles are certainly not a mission-limiting consumable for the Galileo GEM mission.

Thruster valve cycles are somewhat marginal. Table 2 shows the executed number of thruster

Table 2: RPM Engine Summary

As of March 15, 1997	Cycles	On-Time [rein]	Throughput [kg]
21A Thruster	2881	48.47	8.17
22A Thruster	2891	48.64	8.15
Z1B Thruster	1929	33.01	5.64
Z2B Thruster	1929	33.02	5,67
PIA Thruster	12452	211.47	41,06
P2A Thruster	10686	186,25	35,93
LIB Thruster	17685	351.34	67.27
L2B Thruster	17685	292.70	56.93
SIA Thruster	2086	38.65	7,51
S1 B Thruster	275	3.98	0.79
S2A Thruster	1897	37.96	7.45
S2B Thruster	275	4.04	0.80
400N Engine	4	78.01	606.31

pulse cycles for each 10-N thruster as of March 15, 1997. The thruster pulse limit was increased after launch from 23,000 pulses to 35,000 pulses after additional ground tests.' Notice that, as Galileo approaches the end of the nominal mission, the most used thrusters (LIB and L2B) have just barely exceeded half of their allocated thruster pulses. Initial studies of the GEM mission also suggest that not even the L-thrusters and PIA thruster, the most used engines, will reach the consumable limit of 35,000 cycles. PIA thruster usage may be reduced by biasing the trajectory to decrease the likelihood of POSZ clean-up maneuvers or through increased usage of unbalanced turns (either implementation offers propellant savings as well, due to the inefficient nature of the POSZ maneuver and the balanced turn). In summary, thruster valve cycles are also not thought to be a mission-limiting consumable for the GEM mission.

VII. TCM/OTM Summary

Between launch in October of 1989 and March 15, 1997, a total of thirty-eight 10-N and four 400-N maneuvers (including the 2 s wake-up burn) were executed on the spacecraft. Thirteen planned 10-N TCMs/OTMs were canceled due to excellent spacecraft navigation. Of note, two of the Jupiter approach TCMS (TCM-27 and TCM-28) and the first two orbit trim maneuvers following JOI (OTM-1 and OTM-2) were canceled due to a lower-than-originally-planned 10 (gravity assist) flyby coupled with a modification to the orbital tour. Specifically, the first orbit around Jupiter was shortened by approximately one week (one Ganymede orbital period) versus the original design, saving propellant and yet essentially preserving the planned orbital tour after the second Ganymede flyby.

Despite occasional unexplained shifts in 10-N thruster performance (see Chapter VIII), all thirty-eight Galileo 10-N TCMS and OTMS executed well within requirements. It should be stressed that 10-N maneuvers employ a ground-determined burn time that is uplinked to the spacecraft. This is in contrast to main engine maneuvers, which use accelerometer data to close the 400-N pilot valve once the proper Δv is obtained. The 400-N maneuvers also executed well within requirements for ODM, JOI, and PJR (for main engine firings, the requirements pertain to accelerometer accuracy).

For Galileo maneuvers, the best estimate for maneuver performance is obtained from the Navigation Team's Orbit Determination (OD) solution following a maneuver. Table 3 summarizes the delivered performance during all twenty-five trajectory correction maneuvers, up to and including orbit insertion at Jupiter. TCM-25 (ODM) and TCM-29 (JOI) used the 400-N engine; all other TCMS were performed on the 10-N thrusters. The values of Δv displayed in the fourth through sixth columns represent the designed values for the necessary spacecraft velocity increment in the axial and lateral directions, respectively. The next three columns were obtained from OD solutions and represent the executed accuracy ($[\Delta v_{EXECUTED}/\Delta v_{DESIGNED} - 1]*100\%$) during the axial and lateral components, respectively, of each maneuver.

Notice from Table 3 that the delivered execution error has generally decreased with time, as expected given the learning curve associated with modeling the 10-N thrusters. Indeed, the five TCMS with the largest execution errors were the first five performed. A summary of the 10-N TCM statistics is provided at the bottom of Table 3. The 10-N TCM execution error is 10 = 1.09%. Notice also from Table 3 that the 400-N maneuver execution error decreased markedly for JOI versus ODM. It was important to accurately calibrate the accelerometers based on the results of ODM, because the (propellant) cost of fixing JOI underburns or overburns was very significant.

Table 3: TCM Summary Table

	Starting Date	Maneuver Description	Design Dv +Z (m/s)	-Z (m/s)	L (m/s)	Execution Error +Z	-z (%)	L (%)	Total (%)
TCM-1	11/9/89	remove launch bias & 1st Venus target		15.60	1.74	" 0)	1.64	3.29	1.66
TCM-2	12/22/89	2nd & final Venus target	0.16		0.72	2.42		2,17	2,14
TCM-4A	4/9/90	1st Earth-1 target part 1			24.75			-2.30	-2.30
TCM-4B	5/1 1/90	1st Earth-1 target part 2			11.28			-2.17	-2.17
TCM-5	7/1 7/90	2nd Earth-1 target		0.72	0.59		2.48	-0.19	1.39
TCM-6	1 0/9/90	3rd Earth-1 target		0.48	0.19		0.81	-1.59	0.32
TCM-7	11/13/90	final Earth-1 target		1.09	0.67		1.22	1.26	1.46
TCM-8	11 /28/90	TCM-7 cleanup	0.02		0.05	1.23		-0.60	-0.40
TCM-9A	1 2/1 9/90	post Earth-1 cleanup			5.29			-0.25	-0.25
TCM-9B	3/20/91	Gaspra target part 1	0.20		2.27	0.46		0.57	0.53
TCM-10	7/2/91	Gaspra target part 2			3.65			-0.91	-0.91
rcM-11	1 0/9/91	Gaspra target cleanup	0.09		0.34	0.40		0.03	0.01
TCM-12	10/24/91	Gaspra target cleanup		0.05	0.32		0.61	-0.53	-0.55
TCM-14	814/92	1st Earth-2 target		0.41	20.96		2.68	1.30	1.30
TCM-15	10/9/92	2nd Earth-2 target		0.40	0.61		0.36	0.69	0.64
TCM-16	11/13/92	final Earth-2 target			0.89			-0.34	-0.34
TCM-17	11/28/92	post Earth-2 cleanup		0.02	0.02		0.00	-0.01	-0.02
TCM-19	3/9/93	final Ida target		2.12			-0.22		-0.22
TCM-20	8/1 3193	Ida target cleanup		0.07	0.61		-0.36	0.53	0.54
rcM-22	1 0/4193	final probe entry target			38.66			-0.15	-0.15
TCM-22A	2/1 5/94	probe target cleanup	0.09		0.04	-0.18		-0.04	-0.25
TCM-23	4/1 2/95	probe target cleanup	0.05		0.06	-0.32		-0.01	-0.17
3DM	7/27/95	Orbit Defl.(incl. Wake-up Burn 7/24)		61.85			-1.21		-1.21
TCM-26	8129195	1st. (& final) ODM cleanup		0.86	0.44		-0.78	-0.34	-0.65
JOI	12/7/95	Jupiter Orbit Insertion		644.40			0.14		0.14
		Demonstrated 1O-N 1s Execution Error			=		1.0970		

Table 4: OTM Summary Table

	Starting Date	Maneuver Description	Design Av +Z (m/s)	-z (m/s	L	Execution Error +Z	-z (%)	L (%)	Total (%)
PJR	3/1 4/96	Peri-Jove Raise maneuver		377.10	(m , s) "	)	-0.21		-0.21
OTM-4	5/3/96	1st G1 target cleanup		0.45	1.17		0.28	0.07	0.17
OTM-5	6/1 2/96	2nd G1 target cleanup	0.18		0.50	0.14		0.25	0.22
OTM-6	6/24/96	final G1 target cleanup	0.06		0.48	1.00		-0.38	-0.39
OTM-7	6130196	post-G1 cleanup	0.58		0.00	0.30			0.30
OTM-8	8/5/96	G1 to G2 apoapsis maneuver			4.61			-0.45	-0.45
OTM-9	8127/96	1st & final G2 target cleanup	0.00		0.08	0.87		-0.80	-0.80
OTM-11	9/9/96	post-G2 cleanup			5.74			-0.69	-0.69
OTM-12	10/8196	G2 to C3 apoapsis maneuver	0.59		0.11	-0.02		-0.21	-0.05
OTM-14	11/1 0/96	post C3 cleanup			2.33			-0.49	-0.49
OTM-15	11/26/96	C3 to E4 apoapsis maneuver		0.06	0.23		0.61	-0.97	-0.88
OTM-16	12/1 5/96	E4 target cleanup	0.02		0.11	0.97		-0.54	-0.49
OTM-17	12/23/96	post E4 cleanup			1.97			-1.05	-1.05
OTM-19	2/6/97	E4 to E5 apoapsis maneuver	0.21		0.83	0.94		0.21	0.27
OTM-21	2/23/97	post E6 cleanup	0.91			-0.33			-0.33
OTM-22	3113197	E6 to G7 apoapsis maneuver		0.13	15.75		0.77	0.26	0.26
		Demonstrated 1O-N 1σ Execution Error			=		0.46 %		

Table 4 is the analogous OTM performance table to Table 3. The first orbit trim maneuver, OTM-3 (PJR), was the final use of the 400-N engine. Again, accelerometer data dictated the shut-down of this maneuver, with very little residual execution error. 10-N OTM performance (OTM-4 through OTM-22) continues to be excellent, with an execution error 10 = 0.46%. For all 1O-N maneuvers to date, the execution error is 1σ = 0.897.. This demonstrated maneuver accuracy is well within 3σ requirements (LAT = 4.6%, POSZ = 6.0%, PULZ = 3.8%).

VIII. 1O-N Thruster Performance

All maneuvers using the 10-N thrusters are fired in pulse-mode. The Galileo spacecraft (.S/C) is in dual-spin during all 10-N maneuvers except during spin-up and spin-down and all-spin spin corrects. All pulse durations are less than 3 s long, if the thruster is fired once per S/C revolution (about 19s) and 1.5s if fired twice per S/C revolution. The maximum number of pulses fired in a pulse train, called a maneuver segment, is limited to 500 pulses (per thruster). All maneuvers were designed using the Propulsion System Simulation Program (PSSP). PSSP simulates the pressurization system and the propellant tanks as well as the propellant feed system. It also calculates the thrust and mass flow of each engine. PSSP was built empirically from ground test data. It includes a model for each thruster, the main engine, the pressure regulator, the check valves, the propellant tanks, the pressurant tanks and all of the propellant feed lines.

Axial -Z Maneuvers

The so-called PULZ maneuver is executed by firing two Z-thrusters in pulse-mode simultaneously. Depending on the maneuver, the pulses were between 0.57s and 0.93s in duration (the allowed range for PULZ firing is 0.01 s to 0.96 s). During the mission, the number of pulses in a PULZ maneuver segment varied between 4 pulses and 166 pulses per thruster (the allowed range is 1 to 500 pulses).

There are two redundant Z-thruster pairs, one connected to the A-branch and one to the B-branch. The B-branch thrusters are used nominally for the pulsed -Z maneuvers. It was discovered very early in the mission that the Z(B) thrusters impart less spin error to the S/C than the

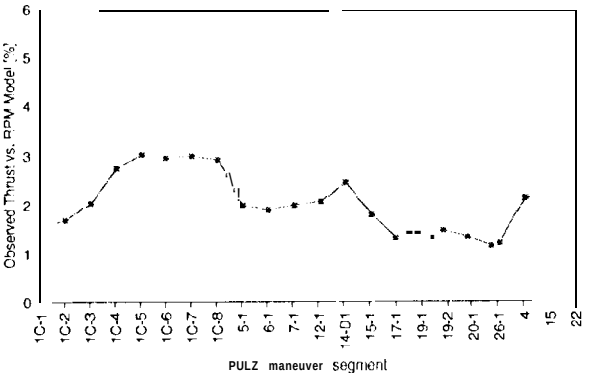

Figure 10: Combined Thrust of Both Z(B) Thrusters During PULZ Maneuvers

Z(A) thrusters, possibly due to differences in thruster misalignment and plume impingement. Since launch we have performed 20 PULZ maneuver segments. The relative thruster performance, i. e., the observed combined thrust of both Z(B) thrusters versus the thrust reconstructed by PSSP using the actual RPM telemetry measurements, is shown in Figure 10. On the average, weighted with the maneuver size, the observed overperformance (versus a ground-test data-based model) is about +2.06%.

The maneuver excursion errors in pointing and spin are illustrated in Figure 11 and Figure 12, respectively. The specific pointing errors are non-directional and therefore counted always positive; they vary between 2.9 mrad and 14.7 mrad per 100 S/C revolutions. This, of course, did turn the Δv direction by about the same angle. The actual maximum error was 7.4 mrad (at TCM-26) versus the requirement to be less than 10 mrad. Most of the attitude disturbing torque is caused by plume impingement effects on the stator, which is held

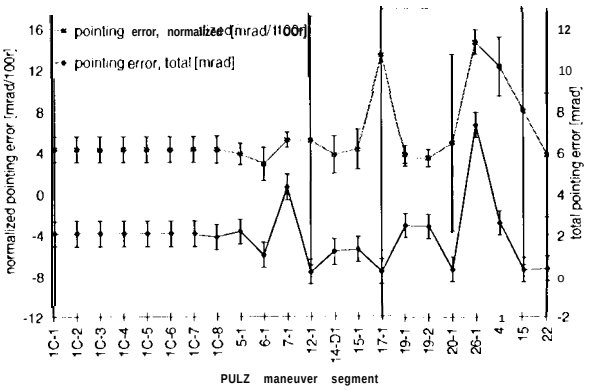

Figure 11: Pointing Excursions During PULZ Maneuvers

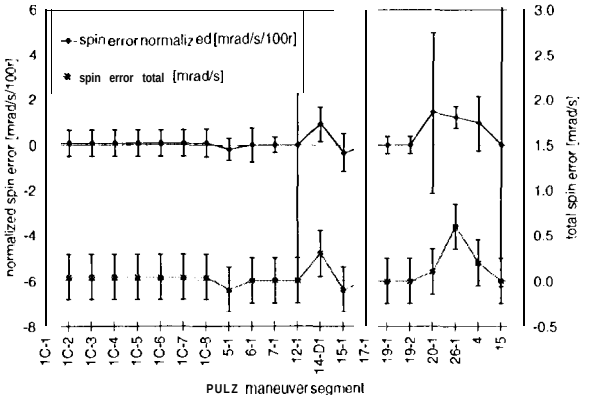

Figure 12: Spin Rate Excursions During PULZ Maneuvers

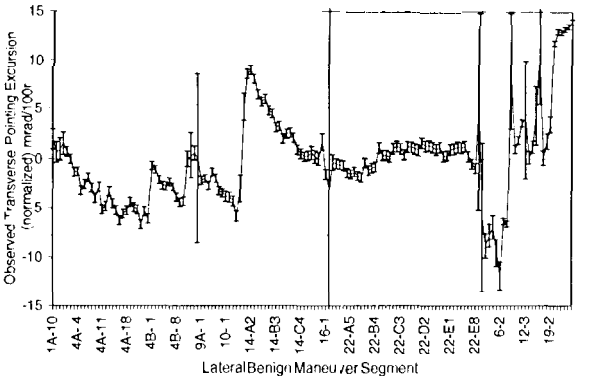

Figure 13: Transverse Pointing Excursions During LAT Maneuvers

inertially fixed. This causes the effective thrust generated by one thruster to be different at one "side" of the S/C versus the other "side." This phenomenon was recognized at TCM-1, about 15 days after launch. The remedy for this was to split larger PULZ maneuvers into an even number of maneuver segments of about equal size. By doing that, the stator could be inertially moved from one side to the other between segments, effectively canceling the attitude excursion generated by plume impingement onto the stator.

From Figure 11 one can deduce that the specific pointing excursions grew from about 5 mrad/100r to about 12 mrad/100r between TCM-20 and TCM-26. The main event during that period was the release of the probe, which was part of the despun section of the S/C.

The spin excursion is required to remain within about ±5 mrad/s. This assures that the thrusters will not be firing outside an allowed burn arc assuming the nominal on-time (a burn arc violation occurs if the spin error is larger than 6.6 mrad/s). An error of this magnitude also equals the capability of one spin correction maneuver. The largest error experienced during any PULZ maneuver was less than 0.6 mrad/s (see Figure 12). The normalized spin excursion was also low, less than 1.5 mrad/s per 100 S/C revolutions.

Lateral Maneuvers (LAT)

The lateral maneuver uses both L-thrusters, firing them alternately one-half S/C revolution apart. Hence, these firings occur in the same inertial direction. Each pulse bit exerts, in addition to the translator impulse, a small y-torque. This causes the S/C to precess around the +x rotor axis. The next pulse, from the other L-thruster, generates a reverse y-torque, turning the S/C back. Lateral maneuvers are designed to effectively zero out all these y-torque bits and minimize the remaining S/C pointing excursion. This is done by adjusting the individual firing times of the two L-thrusters such that their y-torque bits are of equal size. In order to do that, the thrusts and the moment arms of the two L-thrusters have to be calculated in the maneuver design.

Figure 13 shows the resulting specific pointing excursion observed during all lateral maneuver segments executed on Galileo. It turns out that the pointing excursions were significant for most maneuver segments, indicating that the actual thrusts or moment arms were different from the predicted thrusts and modeled moment arms. However, the lateral maneuvers were always broken up into segments small enough to never exceed the pointing requirement of ±41 mrad. The highest total error of 32 mrad occurred in OTM-22, which also had the highest normalized error of 14 mrad/100 r.

There could be also other effects causing these attitude excursions; e. g., a rigid-body model as assumed in the maneuver design does not sufficiently match the actual S/C behavior (propellant sloshing, boom flexing, etc.) or perhaps there could be inaccurate modeling of the mass properties, including the center of mass coordinates (which in turn determine the thruster moment arms). No conclusive explanation has been found to why these y-torque bits are so unbalanced. Not only that, the imbalance seems to have changed throughout the mission. This shift

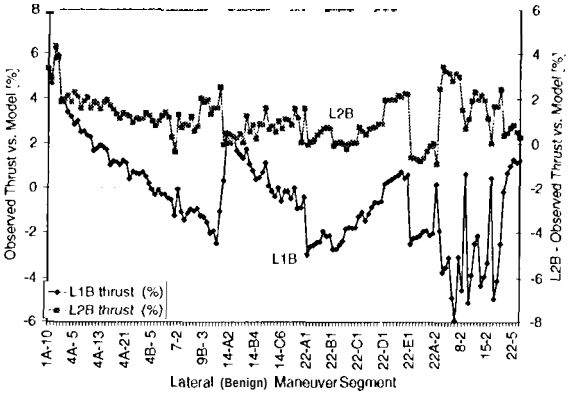

Figure 14: Individual L-Thruster Performance

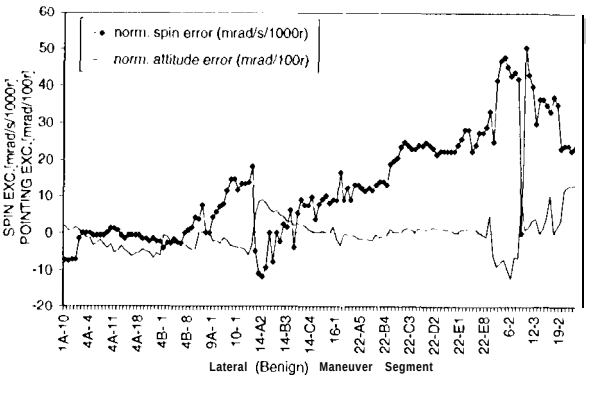

Figure 15: Spin Excursion During LAT Maneuvers (Compared with Attitude Excursion)

has also defied explanation. In our reconstruction, we tested the postulate that the pointing excursions were due to variations in the thrust output, Figure 14 shows how the thrust of the LIB and L2B thrusters have to vary if performance shifts caused all of the observed pointing excursions. The L1 B thruster particularly would have to decrease in its thrust output between launch and the last segment of TCM-10, “recover” in TCM-11, TCM-12 and the first segment of TCM-14, and finally drop again in thrust output to about the same low level as in TCM-1O. In order to minimize maneuver errors, the PSSP database was adjusted several times throughout the mission. The overall maneuver-size weighted performance of the L1 B thruster versus the (ground-test data-based) model is -0.38%, with a standard deviation of 2.2%. The L2B thruster performance is much tighter; the data 1σ is only 1.0% and the average overperformance is +1.1 O%.

The spin rate excursions during all lateral maneuver segments were small, except during TCM-22. For some reason, the pointing errors during that maneuver were negligible, but the spin errors were significant. This was typically the case—lateral thruster pointing and spin excursions generally behaved reciprocally.

Figure 15 shows the normalized spin excursions throughout all lateral maneuvers. The most remarkable part of the figure is that both the pointing excursion as well as the spin error changed direction between TCM-11 and TCM-12 (91 -282 and 91-297). This is so distinct that it suggests that an unmodeled change in the S/C mass properties may have caused a shift in the S/C’s center of mass.

The error of the center of mass between model and flight necessary to cause the observed spin and pointing excursions is shown in Figure 16. The error in y-axis is solely determined by the observed spin error, and the error along the z-axis is driven by the observed pointing error. Unfortunately, no mechanism could be identified resulting in an error of the center of mass depicted in Figure 16. In addition to that, most changes in the real S/C mass properties would also show up in the wobble. However, no significant unexplained wobble changes have been observed,

It should be noted that the large attitude excursions and the related spin excursions are definitely systematic and not statistical. However, no definite cause could be identified, but several candidates are viable: (1) flexible S/C element model errors (propellant sloshing, boom flexing, etc.) versus rigid body models; (2) inaccurate modeling of the S/C center of mass location; or (3) actual shifts in thruster output.

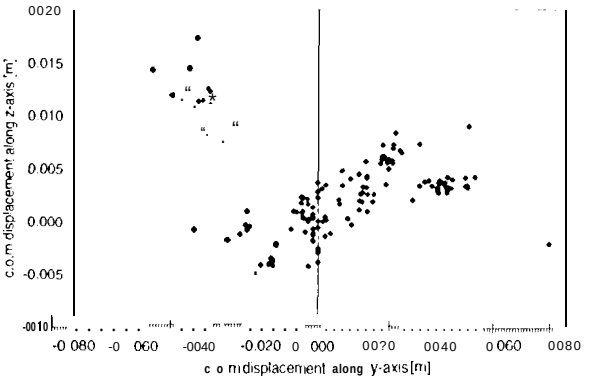

Figure 16: Postulated Error in S/C Center of Mass

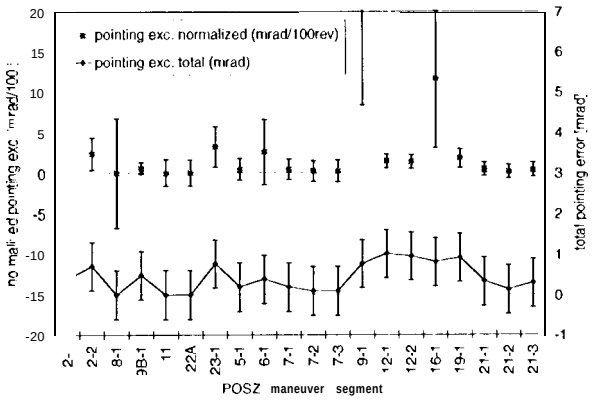

Figure 17: Pointing Excursions During POSZ Maneuvers

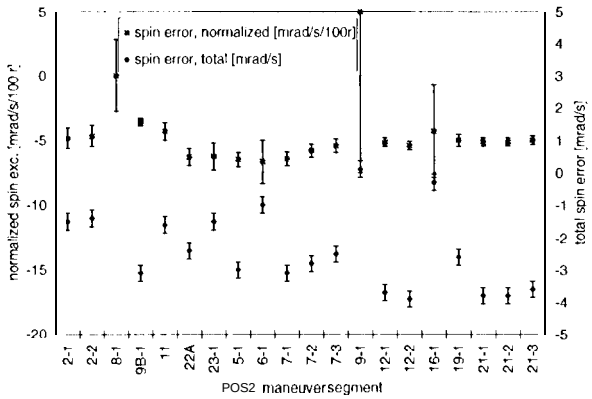

Figure 18: Spin Excursions During POSZ Maneuvers

Axial +Z Maneuvers

The POSZ maneuver uses only one thruster. The PIA thruster fires twice per S/C revolution, one-half S/C revolution apart. The on-times for both pulses are the same, effectively canceling the lateral Δv component and also the y-torque bits. Ideally, there should be no effect on the pointing of the S/C during POSZ firings.

In fact, the normalized pointing excursion was less than 3.2 mrad/100 r during all POSZ maneuvers except for OTM-9 and OTM-16, the two smallest POSZ maneuvers (accordingly, these had the largest uncertainty in determining the actual pointing excursion; see Figure 16). The next worst specific pointing excursion of 3.2 mrad/100 r occurred at TCM-23. With a pointing requirement of 10 mrad, the segment size was limited to about 300 S/C revolutions. The maneuver-size weighted average pointing excursion was 0.97 mrad/100 r. The actual total pointing errors were less than or equal to 1 mrad for all POSZ segments, well within the pointing requirement of 10 mrad for POSZ maneuvers.

The actual total spin excursions (Figure 18) were between O mrad/s and -4 mrad/s, which is within one spin correction capability of ± 5 mrad/s. The weighted average for the normalized spin errors were 5.2 mrad/s per 100 r. There are no burn arc violations until the error reaches 81 mrad/s; however, a spin rate monitor in the AACS software trips whenever the spin rate changes by more than 33 mrad/s.

The thrust model in the propulsion software was modified to closer match the observed thrust performance. The Δv-weighted overperformance is 4.57% compared to the original ground test data. The relative overperformance for each maneuver segment is shown in Figure 19. There has been no observation of any thrust degradation.

P-Thruster Turns

The performance of the P-thruster couple or A-branch Z-thruster couple during balanced and unbalanced spacecraft turns, respectively, may be determined from RPM and AACS data. Unlike TCMS and OTMs, spacecraft turn maneuvers do not fire a commanded number of thruster pulses. Rather, an AACS control algorithm ceases thruster firing when the correct spacecraft attitude has been obtained. Therefore, a thruster overperformance (versus ground test levels) would show up as a reduced number of thruster pulses, not as an overshoot of the targeted inertial attitude.

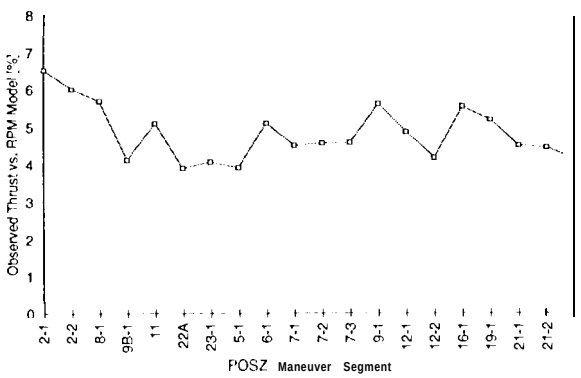

Figure 19: Relative Thrust Performance of PIA Thruster During POSZ Maneuvers

The average thrust of the P-thruster or A-branch Z-thruster couple may be determined by examining the attitude change of the spacecraft during the maneuver, together with the relevant spacecraft properties (e.g., spin rate and rotor moment of inertia). This observed thrust for the thruster couple may be compared with the modeled thrust level for the couple to determine the relative performance of the thruster pair. It should be mentioned that the individual performance of each P-thruster or A-branch Z-thruster is not discernible from this process.

Over 200 P-thruster maneuvers were analyzed to determined the performance of the P-thruster couple versus ground test levels. This analysis includes all balanced turns and sun acquisitions between launch and March 15, 1997. It was determined that the P-thruster couple overperformed by an average level of +4.9% versus pre-launch levels. This number has been reduced from a value of +6.5% obtained previously; an error was found in the prior analysis.' Even with this reduction, it appears that the P-thrusters are overperforming more than any of the other 10-N thrusters. Moreover, the average performance level has shifted very little (<0.2?'.) throughout the mission, in contrast with postulated in-flight L-thruster performance shifts (>5%).

Figure 20 charts the P-thruster performance during the 201 turn maneuvers, viewed as a function of the executed turn angle of precession. It may be noted from the figure that large deviations from the (turn angle-weighted) average overperformance of +4.9% occur only for small turns. This is as expected, since the relative contribution of the attitude uncertainty is more dominant for smaller turns.

The high overperformance of +4.9% for the P-thruster couple is excellently corroborated by the inferred overperformance of +4.6% for the PIA thruster during POSZ maneuvers, mentioned above. No other thruster has averaged as high of an overperformance during TCMs/OTMs. Given an overperformance of +4.6% for the P1A thruster and +4.9% for the P-thruster couple, this requires an overperformance of +5.2% for the P2A thruster. This is not at all hard to imagine, and the resulting (slight) torque imbalance in such a case would generally not be visible to the Galileo Navigation Team during balanced precession maneuvers. Uncertainties in the P-thruster plume impingement losses and thruster misalignments further cloud attempts to determine the individual thrust levels for the PI A and P2A thrusters during precession maneuvers.

n-Branch Z-Thruster Turns

Between launch and March 15, 1997, a total of twenty-six unbalanced turns were performed on the Galileo spacecraft. Unbalanced turns offer many advantages versus their balanced counterparts, including: smaller pointing and spin excursions, two-thirds less propellant usage, more equal division of 10-N thruster usage, better thruster thermal characterization (since the Z2A temperature transducer has not failed), less turn-time required, etc.' All twenty-six unbalanced turns were analyzed to determined their relative performance versus ground test levels.

Figure 21 displays the A-branch Z-thruster couple overperformance, viewed as a function of the executed turn angle of precession. The (turn angle-weighted) average performance for all unbalanced turns is +3.3%, again representing an

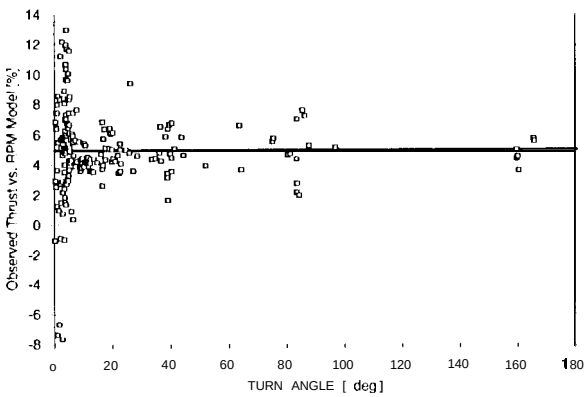

Figure 20: P-Thruster Performance vs. Turn Angle

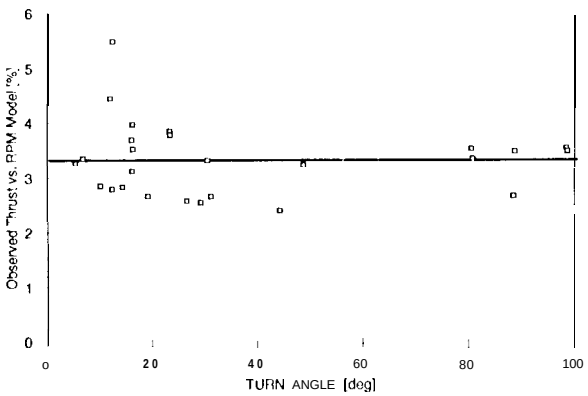

Figure 21: Z-Thruster Performance vs. Turn Angle

overperformance versus ground test levels. Compared with the balanced turns, unbalanced turns appear to be more repeatable (with respect to average overperformance).

The only other A-branch Z-thruster maneuvers that were analyzable in the Galileo mission were the first two (PULZ maneuver) portions of TCM-1, just 15 days after launch in 1989. The average overperformance values determined for these two TCM-1 segments were +0.1 % and +1 .5%, somewhat lower than the +3.3% average found for unbalanced turns. This is perhaps not surprising, since each Z-thruster fires twice per S/C revolution in a PULZ maneuver, while each Z-thruster only fires once per revolution during unbalanced turns. Hence, the performance differences may be due to differences in plume impingement between the two sides of the spacecraft at which the Z-thrusters are fired. Also, it should be noted that TCM-1 utilized NTO and MMH that were not yet fully saturated with helium; it is known that the performance level is lower for unsaturated versus saturated propellants.

S-Thruster Maneuvers

A complete analysis of S-thruster maneuvers (thruster flush, spin correction, spin-up, and spin-down maneuvers) between launch and March 15, 1997, was undertaken. The S1 B and S2B thrusters (backup S-thrusters) have only been used in thruster flush maneuvers (which fire two pulses each), while the S1 A and S2A thrusters (primary S-thrusters) have been used during thruster flushes, spin corrections (again, firing two pulses each), and most extensively in large spin-up/spin-down maneuvers.

A total of five spin-up and five spin-down maneuvers were executed on the S2A and S1 A thrusters, respectively. These large spin-rate change maneuvers were executed for spin-up/spin-down demonstration, probe release, ODM, JOI, and PJR (in chronological order). Typically firing 300-400 pulses, these maneuvers offered the best characterization of S-thruster performance during the Galileo mission. Future S-thruster usage is expected to be minimal.

SIA Thruster

A total of 136 SIA thruster maneuvers between launch and March 15, 1997 were investigated; in fact, all maneuvers amenable to analysis were included. Some spin corrections and many thruster flushes were not analyzable—the spin corrections due to lack of spacecraft data while at a large off-Earth attitude, and the thruster flushes due to a lack of time resolution for a new, less time-consuming thruster flush sequence utilized since 1993. However, continuing frequent spin corrections and the five spin-down maneuvers have allowed a much more thorough S1 A thruster performance characterization than was possible four years ago.'

Figure 22 displays the SIA thruster performance versus ground test levels as a function of the thruster on-time (per pulse). No distinction is made between short and long pulse trains in this plot. A constrained exponential fit of the data of Figure 22 was made, since it is known from ground test data that below an on-time of approximately 0.6 seconds, the performance starts to drop off (the "pulse-mode" effect). Comparisons between ground test data anti the exponential fit of Figure 22 show that the in-flight pulse-mode effect is consistent with expectations.

Notice also from the figure that the asymptotic value of the overperformance is very nearly +4% versus ground test models. In fact, the average of all 101 data points with an on-time greater than 0.6 seconds (an approximate point where the operation may be considered "steady-state") is +4.0%. The large spread in the flight data is not surprising, given the very limited spin rate change imparted to the spacecraft during thruster flushes and spin corrections, and hence the large associated uncertainty in the change in Galileo's spin rate during these maneuvers.

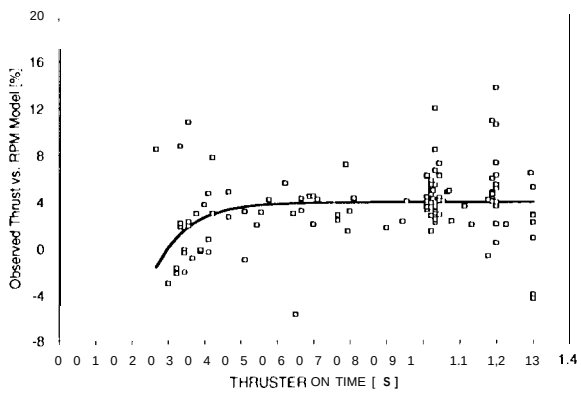

Figure 22: SIA Thruster Performance vs. On-Time

The average overperformance during the five spin-down maneuvers, arguably the "best" numbers for SIA thruster performance, are quite a bit lower than average value of +4.0% determined above. Specifically, the five spin down maneuvers displayed the following overperformance values: demonstration, +2.2%; probe release, +2.8%; ODM, +0.9%; JOI, +2.8%; and PJR, +1.7%. Incidentally, the first four spin-down maneuvers utilized a thruster duty cycle of 1.3 seconds on/3.9 seconds off, while the PJR spin-down employed an alternate duty cycle of 0.9 seconds on/0.9 seconds off. This was necessary due to propellant unporting concerns near the end of PJR. Duty cycle dependency for these five maneuvers should be of little consequence, since thruster on-times above 0.6 seconds are essentially steady-state.

The reason that the five large spin-down maneuvers underperform versus other SIA thruster maneuvers (spin corrections and thruster flushes, which require only two pulses each) is unknown. However, it is possible that it is related to a temporary, minor reduction of 10-N film cooling, a phenomenon that was observed in the time traces of the S1 A temperature transducer during all five spin-down maneuvers. Figure 23 shows all five S1 A thruster temperature transducer traces during spin-downs. A minor thermal rise may be seen during each of the five spin-down maneuvers. This result was not unexpected, since ground test data showed some very similar thermal characteristics of the same thruster when fired at these most thermally stressful duty cycles (1.3 seconds on/3.9 seconds off or 0.9 seconds on/0.9 seconds off). In fact, the five spin-down maneuvers remain the only examples of any reduction of 10-N thruster film cooling observed in

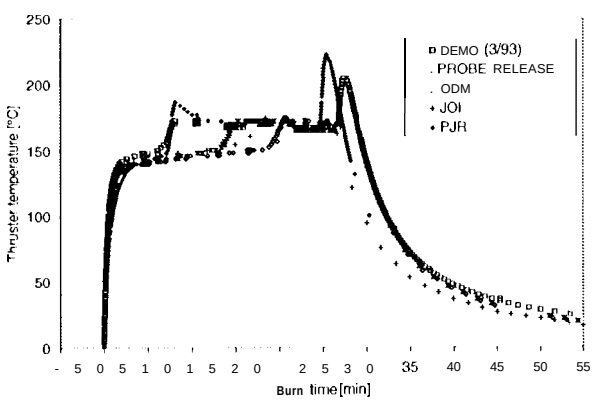

Figure 23: SIA Thruster Temperature During Spin-Down Maneuvers

the Galileo mission. This is also not surprising, given the curtailed operating range employed by the Galileo 10-N thrusters, as well as the quite benign duty cycles used for all other types of 10-N maneuvers in flight.

Further evidence corroborating the above explanation for the relative underperformance of the large versus small SIA thruster maneuvers may be found by studying the S2A thruster, used for spin corrections, thruster flushes, and large spin-up maneuvers. Specifically, no differences in S2A thruster performance were noted for large versus small maneuvers, unlike the SIA thruster. Moreover, no loss of film cooling was noted for any S2A thruster burn, also unlike the S1A thruster. It is quite conceivable that the temporary reduction in film cooling during the five large spin-down maneuvers caused an additional 1-30/. decrease in the SIA thrust versus smaller maneuvers. This had no operational impact—in fact, the spin-rate "overshoot" was actually reduced in these five cases, since the spin-up and spin-down algorithms are essentially open-loop.

S2A Thruster

A total of 108 S2A thruster maneuvers between launch and March 15, 1997 were investigated; in fact, all maneuvers amenable to analysis were included. As before, some spin corrections, and all thruster flushes after 1993 were not analyzable. Continuing frequent spin corrections and the five spin-up maneuvers also have allowed a much more thorough S2A thruster performance characterization than was possible four years ago.'

Figure 24 displays the S2A thruster performance versus ground test levels as a function of the thruster on-time (per pulse). No distinction is made between short and long pulse trains in this plot. Similar to the SIA thruster, comparisons between ground test data and the exponential fit of Figure 24 show that the in-flight pulse-mode effect is consistent with expectations.

Notice also from the figure that the asymptotic value of the overperformance is +2.5% versus ground test models. The average of all 86 data points with an on-time greater than 0.6 seconds is +2.6%; this is the appropriate number to use for an average performance value for the S2A thruster. As before, the large spread in the flight data is not

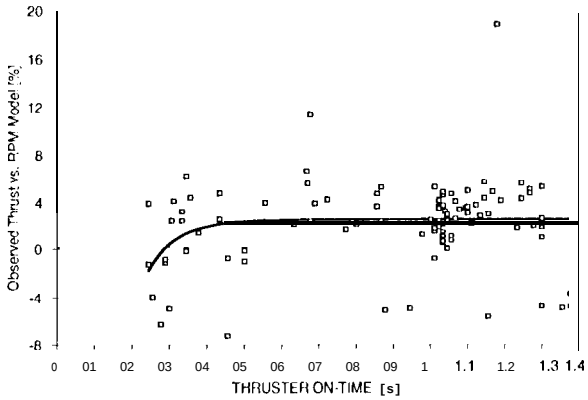

Figure 24: S2A Thruster Performance vs. On-Time

surprising, given the very small spin rate change imparted to the spacecraft during thruster flushes and spin corrections.

S1 B and S2B Thrusters

As mentioned previously, both B-branch S-thrusters have been used in thruster flushes only, kept healthy in the unlikely event that they would need to replace a failed A-branch S-thruster. All thruster flushes between launch and early 1993 were analyzed to determine B-branch S-thruster performance. No performance assessment was possible after early 1993, given a change to the standard thruster flush sequence, mentioned above.

A duty cycle dependence assessment is impossible for the S1 B and S2B thrusters, since thruster flushes only used a very limited on-time range of approximately 0.9-1.3 seconds. This range is essentially equivalent to steady-state, so all 58 S1 B and 60 S2B data points obtained were used in determining steady-state averages.

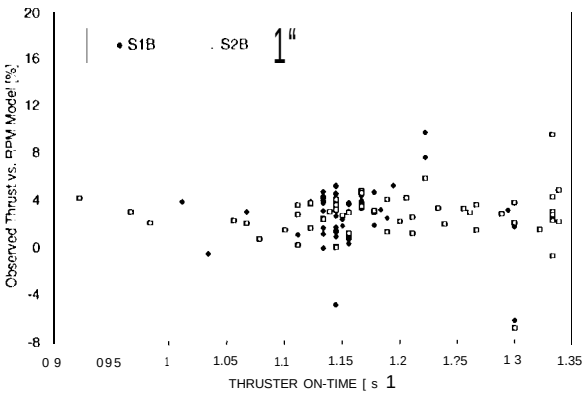

Figure 25: S1 B/S2B Thruster Performance vs. On-Time

Table 5: 10-N Thruster Performance Summary

IO-N Thruster	Number of Data Samples	Performance VS. Ground Test (average * lfs)
L1B	147	-0.38% * 0.17%
L2B	147	+1.10% * 0.07%
Z1B & Z2B	22	+2 06% ± 0.13%
P1A (POSZ)	20	+4.57% * 0.13%
PIA & P2A (TURN)	201	+4.89%± 0.11%
Z1A & 22A (TURN)	26	+3.29% * 0.05%
S IA	101	+4.02%± 0.27%
S2A	86	+2.63%± 0,36%
S IB	58	+2 82% ± 0.42%
S2B	60	+2 54% ±0.26%

Figure 25 displays the S1 B and S2B overperformance data as a function of thruster on-time" per pulse. Note from the figure that the S1 B and S2B thruster data sets are quite complementary, and that there is no detectable duty cycle dependence for either thruster over this on-time range (as expected). The average S1 B overperformance is +2.8%, only slightly different than the S2B average overperformance of +2.5%. This is very much within the observed flight range for the other 10-N thrusters, demonstrating some general consistency in 10-N overperformance versus ground test levels.

10-N Thruster Performance Summary

Table 5 represents the best estimate for the 10-N thruster performance during all analyzed 10-N thruster activities through March 15, 1997. Performance estimates of the Galileo 10-N thrusters are vital to characterize the engines, since maneuver firing durations are determined a priori (e.g., they are not governed by accelerometer cut-off). The 1 σ errors stated in the table represent the calculated standard deviation of the average value for the different maneuver reconstructions. Therefore, small values for CT correspond to large sample sizes and/or small in-flight demonstrated variability.

Notably, Table 5 displays strong evidence for a generally consistent overperformance of a few percent for all 1O-N thrusters versus ground test levels. The reason for this general 10-N thruster overperformance is not known; however, it is conceivable that a systematic error in the 10-N thrust stand in Lampoldshausen, Germany, could explain the trend. In fact, if the impulse bits determined at Lampoldshausen being under-reported by 2.8%, this minimizes the statistical spread in the flight data versus ground test levels

(if it is assumed that all Galileo 10-N thrusters are performing the same in flight as in ground test).

However, it was earlier shown that there may have been a statistically significant shifts in L-thruster performance during the Galileo mission. Therefore, the inclusion of the L-thrusters in the above assessment is suspect. Excluding the L-thrusters, the statistical variation in the flight data is minimized assuming that the impulse bits measured at Lampoldshausen are being under-reported by 3.50/.. Whether or not the L-thrusters are included, either interpretation is potentially a significant finding which may have implications for future testing in the 10-N thruster test stand for other projects.

IX. 400-N Engine Performance

Table 6 lists all the important parameters for all 400-N burns, including 1σ error bounds. It also gives some information on how the different parameters were derived. The specific impulse was interpolated from measured ground test data. After the ODM in July, 1995, the 400-N model (in the PSSP software) was updated to match the observed performance. In particular, the thrust turned out to be about 1.8% lower than modeled in PSSP for ODM reconstruction. The ground test data suggested that the original model overestimated the specific impulse (Isp) by about 0.59'.. The remaining error was attributed to an overprediction of the total mass flow by about 1.3%. The reconstruction of the subsequent JOI Maneuver as well as the PJR Maneuver confirmed the same discrepancy between the actual performance and the original model.

The Orbiter Deflection Maneuver was executed on July 27, 1995. Three days prior, a small two-second burn (see Chapter V) was executed to verify the proper engine operation after the engine was "stored" for six years inflight. Two seconds were enough to detect and identify any conceivable failure modes without risking much propellant (or the spacecraft) in case there was a functional problem. The thrust output was about 10% lower than during the first 2 s of any of the subsequent 400-N usages. This phenomenon was attributed to the fact that the propellant feed lines (a few meters in length) were wetted only a week before the wake-up burn, and some helium gas and propellant froth (generated during the line

Table 6: Summary of ODM, JOI and PJR

Parameter	ODM	JOI	PJR	derived from
POX [bar]	16.80 +/-0.10	16.30 +/-0. 10	16.80 +/-0. 10	from RPM telemetry
PFU [bar]	16.95 +/-0.10	17.14 +/-0.10	16.33 +/-0. 10	from RPM telemetry
TOX ["C]	16.5 +/-0.7	130 +/-0.7	14.4 +/-0.7	from RPM telemetry
TFU ["C]	17.0 +/-0.7	14.0 +/-0.7	14.7 +/-0.7	from RPM telemetry
$T_{coolant}$ ["C]	71 +/-3	65 +/-3	71 +/-3	estimated from ground tests
MR [1]	1.67 +/-0.01	1.62 +/-0.01	1.71 +/-0.01	from PSSP
Isp [s]	307.6 +/-1.8	306.7 +/-1.8	307.4 +/-1.8	based on ground tests
F [N]	3950	388.6 +/-0.6	391.8 +/-1.1	from ΔI and Δt
At [s]	306.13 +/-0.03	29140,40 +/-0.03	1480227 +/-0.03	from AACS telemetry
I [Ns]	121725	1142414 +/-1874	560371 +/-1510	from mi, Δv and Isp
ṁ [g/s]	131.0	129.2 +/-0.7	130.0 +/-1.0	from Δm and Δt
m_i [kg]	2012.2	1996.72 +/-3.0	1588.1 +/-3.6	from ground records
Δv [m/s]	61.11	645.23 +/-0.2	376.29 +/-0.02	from Navigation
AmOX [kg]	25,2	234.9 +/-1.4	117.3 +/-1.0	from Δm and MR
ΔmFU [kg]	151	144.9 +/-1.0	68.6 +/-0.6	from Δm and MR
Am [kg]	404	379.8 +/-2 1	185.9 +/-1.5	from mi, Δv and Isp

filling process) were still present in the propellant lines.

The wake-up burn was fixed to be exactly 2 s. For greater accuracy, the ODM burn was accelerometer controlled. The imparted Av was 1.2% low, since the accelerometers were not yet in-flight-calibrated for a 400-N maneuver.

The largest maneuver was JOI. The 400-N model as well as the accelerometer calibration were updated based on the observations at ODM. JOI was cut off as planned by the accelerometers, leaving an eXeCUtiOn error in Av Of +0.1 3%. Reconstruction revealed that the 400-N performance was about 0.6% lower than predicted by the RPM model (which was updated after ODM). This was mainly due to the anomalous behavior of the oxidizer side check valve in the pressure control system of the RPM. The amount of the pressure drop across the oxidizer check valve could not be predicted very well for JOI because of the short burn duration at ODM.

The final 400-N maneuver (PJR) was carried out on March 14, 1996. It was about half the size of JOI. The execution error again was determined

by the performance of the accelerometer. The Av fell short by about 0.2%. The thrust output, however, was 0.8% lower than expected due to another anomaly. The fuel side check valve did not pass sufficient helium gas to keep the regulated pressure at the expected level. This behavior was a new development following JOI, where there was no indication of a flow restriction in the fuel side check valve.

X. Pressurization System

Shortly after launch in October, 1989, the propellant tanks were pressurized by firing a set of pyro valves, putting the prime pressure regulator on line. Then the combined pressure regulator and check valve operation consisted of subsequent filling and lock-up events, which were caused by propellant expulsion and tank temperature variations. Sometimes the regulator or check valves did not lock up completely but continued trickling helium over months. This "fine regulation mode" should not be confused with leaking, because it occurred without raising the tank pressures (this was possible due to propellant consumption or slowly decreasing tank temperatures). No leak or degradation could be detected until the pyro valve PC17 (see Figure 6) was fired to prepare for 400-N engine operation. This valve pressurized the engine valve and was fed by the line between pressure regulator and check valves. The propellant tank pressures were such that a cracking of the fuel but not the oxidizer check valve was expected. However, propellant tank filling occurred on both sides. Other evidence from the ODM burn suggested that the oxidizer check valve might have lost its reseat pressure or even became stuck open; however, unknown absolute tank pressure values (due to pressure transducer drift) clouded this determination.

The uncertainty in the state of the oxidizer check valve levied a particular challenge on the flight team between ODM (July, 1995) and post-PJR (April, 1996); namely, to keep tank pressures and temperatures nearly constant to avoid any chance of opening the fuel check valve and forcing oxidizer vapor (and any condensed NTO) into the MMH tubing and MMH tanks. The main heat sources for the tank structure are the power bus regulator shunts. Therefore, temperature control translated into control of power consumption, which affected the entire operation of the spacecraft.

Since the power requirements for the orbital tour post-PJR and the effort to keep tank temperatures constant were incompatible, the decision was made to capture the tank pressure state immediately after the F'JR burn by isolating the pressure regulator. From previous experience (ODM and JOI), a positive pressure difference between the MMH and NTO tanks was expected, which mitigates vapor transport between the tanks. However, a MMH check valve malfunction during PJR (see later this chapter) reversed the tank pressure difference. Fortunately, an observable leak did not occur and one of the check valves apparently held the pressure difference. But the dilemma between power and temperature control still existed. Careful assessment of the situation showed that it would be safe to raise the tank temperatures to the operational levels required in the tour. Because the pressurant tubing was flushed with helium by the previous burn, even if pressure equalization of the NTO and MMH tanks would occur, it would not be catastrophic. Furthermore, the risk of a reaction between NTO and MMH would have increased with time due to diffusion and condensation of NTO vapor in the tubing. In April, 1996 the power margin and thus the tank temperatures were raised to a level which would not be exceeded for the rest of the mission. Subsequently the lower (and variable) operational power margin for the orbital tour was established. Now there is good data post-PJR, following regulator isolation, that suggest that the oxidizer check valve must be closed. This means that the vapor transport threat never existed.

The pressure regulator performed perfectly throughout the mission. As indicated by the helium and propellant tank pressures, the reconstructed regulator characteristic (downstream pressure versus upstream pressure and helium flow rate) during 400-N burns reflected the pre-launch ground measurements. Although the downstream pressure is not accessible via direct measurement, this information could be derived from the combined NTO and MMH check-valve behavior. Except for some variations in the early mission after pressurization, the cracking and lock-up pressure history demonstrated the expected shift versus the upstream pressure.

A lock-up always had to be induced by thermally raising the tank pressures. If not forced to lock up, the soft-seat regulator demonstrated its remarkable ability to keep the output pressure at

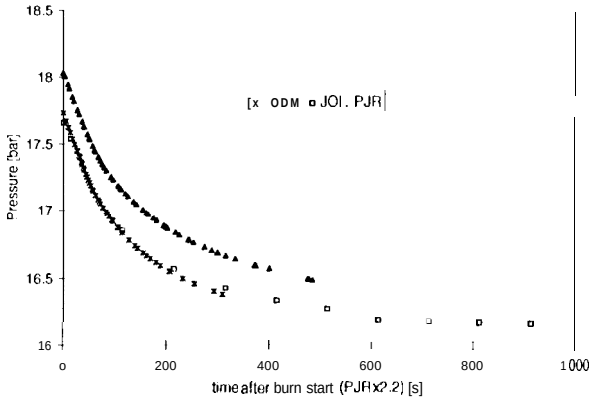

Figure 26: NTO Tank Pressure During ODM, JOI and PJR

an almost constant level over months in a fine regulation mode. It opened and closed many times during such periods but it never really locked up. The ullage increase caused by thruster flushes and other small 10-N maneuvers was compensated with exceedingly low helium flow rates.

However, during 400-N burns, restricted helium flow through the check valves resulted in larger than anticipated pressure drops in both the oxidizer and fuel tanks. By comparing the blow-down and regulated portions of the three 400-N burns (see Figure 26 and Figure 27), only the MMH tank pressure during JOI indicated a nominal behavior; i.e., a pure blow-down portion followed by a constant-pressure regulated portion. The slight up-shift is an expected regulator response to the decreasing helium tank pressure.

The oxidizer check valve showed a flow restriction during all **400-N** engine maneuvers,

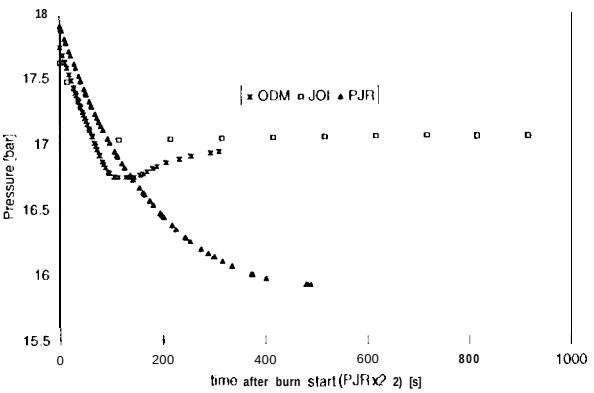

Figure 27: MMH Tank Pressure During ODM, JOI and PJR

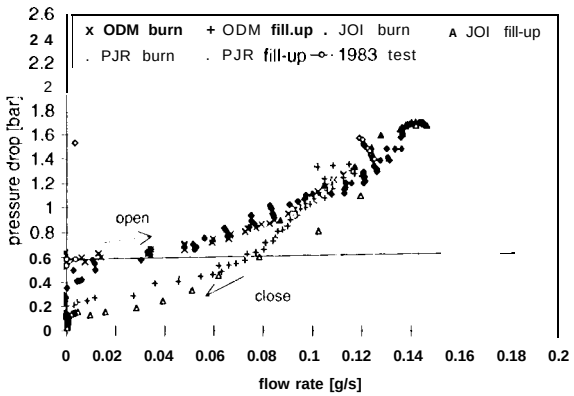

Figure 28: NTO Check Valve Characteristic

having a characteristic similar to a fixed orifice. Although the reseat pressure may have been zero (depending on the assumed downstream pressure, which is unknown due to pressure transducer drift), the data showed an existing cracking pressure and evidence of a nominal checking function. From Figure 28, which represents the pressure drop across the check valve versus the helium flow rate on the oxidizer side, the check valve performed repeatably for all three maneuvers. The hysteresis between the "open" characteristic, as the helium flow increases, and the subsequent "close" characteristic post-burn demonstrates the difference between cracking and reseat pressure. The line in Figure 28 represents the ground test of the NTO check valve in 1983; one "anchoring" data point is off-scale to the right.

The fuel check valve performance was different during each 400-N maneuver. Figure 29 (and also the MMH tank pressure, Figure 27) illustrates this remarkable change in characteristic. At ODM it showed high cracking pressure, then opened wider than required ("overshoot") and

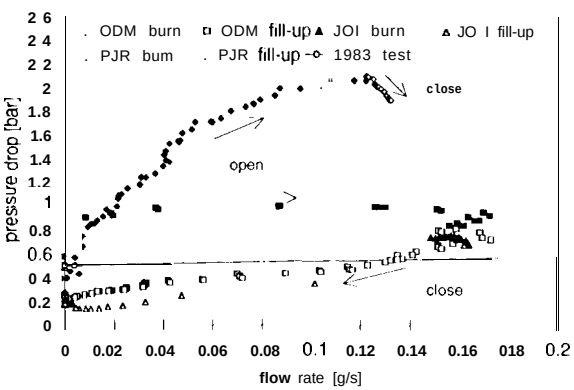

Figure 29: MMH Check Valve Characteristic

eventually delivered the required helium flow rate at a nominal pressure drop. At JOI the check valve showed a nominal performance (regarding cracking pressure and pressure drop at full helium flow), similar to the ground test data. At PJR it was flow-restricted similar to the oxidizer check valve. In fact, the flow restriction was even worse than on the oxidizer side and the characteristic indicates that the check valve was slowly opening throughout the maneuver, rather than being a fixed orifice. This caused the fuel tank pressure to decrease throughout the burn and end up 1.5 bar lower than predicted, a large discrepancy.

The heat transfer from the liquid propellant components and the tank walls into the ullage gas was significant during changes in temperature and pressure. The polytropic coefficients (n)—based on dynamic tank models and pressure/temperature telemetry-were calculated for the helium tank depletion as well as for the propellant tank blow-down phases. For the NTO and MMH tanks, the polytropic coefficients were determined to be 1.18 and 1.40, respectively. For the helium tank a varying polytropic coefficient was found (ODM: 1.3, JOI: 1.3-1.22, PJR: 1.16), dependent on the helium mass. Low helium tank outlet temperatures (as low as -23 'C) caused no concerns for the propellant components, because mixing with the ullage gas and the above mentioned heat transfer sufficiently limited the cooling effect on the gas in the propellant tanks.

Propellant vapor effects were apparent only in the NTO tanks. On the oxidizer side, the polytropic coefficient during blow-down was lower compared to the fuel tank due to the condensation heat of NTO vapor. Post-burn, after the helium flow fill-up was completed, a subsequent slow vapor pressure buildup caused the oxidizer tank pressure to increase further compared to the fuel side. Vapor pressure effects were even apparent during changes in tank temperatures after pressure regulator isolation, where the vaporization/condensation heat of NTO increased the heating/cooling time constant of the oxidizer tank compared to the fuel tank.

The performance of the pressurization system was evidently affected by some hardware degradation that caused highly restricted flow of helium through the oxidizer and fuel check valves during 400-N engine firings. Analysis of the launch pressurization data suggests that the full required flow of helium through each check valve (of up to 0.16 g/s , necessary for 400-N engine burns) could be easily supported. Therefore, the inability of the check valves to provide the required helium flow, especially with first the oxidizer and then fuel check valve being affected, suggests that NTO may have, over time, caused some hardware degradation in the oxidizer check valve, and possibly in the fuel check valve. Pure NTO vapor exposure of Galileo spare check valves in ground tests has shown a similar increase in cracking pressure and flow restriction. Significantly, the tests revealed that many months of oxidizer exposure were required to produce the check valve seal swelling believed responsible for the behavior of the NTO check valve; compatibility testing during development was of an inadequate five-day duration. Table 7 lists our in-flight observations reconstructed from Galileo telemetry, encompassing different pressure transducer drift scenarios (see chapter XI) as well as all the main events (PC17 firing, ODM, JOI, PJR). The very right column compares this to the test results. Note the large discrepancies in the dP parameters, apparently due to NTO exposure.

Table 7: Check Valve Parameters

	OX CV [bar]	FU CV [bar]	TEST CV [bar]
cracking dP	0.0 to 0.7	0.6 to 1.2	0.4 to 3.5
reseat dP	0.0 to 0.7	0.2 to 0.6	0.0 to 0.3
flowing dP	1.5 to 1.7	0.5 to 2.4	0.7 to 2.3
	(@0.15 g/s)	(@0.13 g/s)	(@0.14 g/s)

However, there is no indication that the pressure regulator might have changed its characteristic over more than six years of operation until it was isolated. The device evidently performed excellently in regulation and lock-up modes and mirrored the ground tests throughout the mission.

XI. Pressure Transducer Drift

The helium, NTO and MMH tank systems are equipped with a total of seven pressure transducers. On each propellant component, two transducers are connected to the "gas" side (NTO: PO1, P02; MMH: PF1, PF2) of the tanks and an additional one is connected to the propellant feed line upstream of the latch valves (NTO: P03; MMH: PF3). Only one transducer is used to measure the helium tank pressure (PH1).

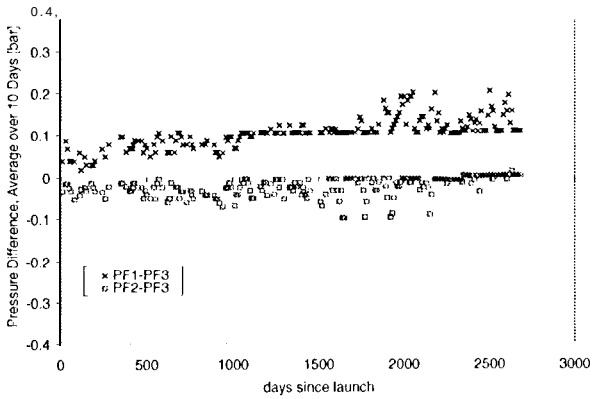

Figure 30: MMH Pressure Transducer Drifts

Ideally all three pressure channels of a propellant component should read identically except during maneuver periods, during which the line pressure may be different from the tank pressure due to propellant flow. By investigating the relative difference between any two of the three redundant pressure telemetry channels over time, offsets and relative drifts were found on both the NTO and MMH side. Whereas the relative offsets of the MMH transducers at launch and the relative drifts over seven years were about 1 DN (Data Number: digital unit = 0.09 bar, see Figure 30), the NTO side revealed considerably larger values (Figure 31). At launch the differences PO1 - P03 and PO2-PO3 were more than twice as large as the largest MMH transducer offset. Also the relative drift rates of PO1 versus P02 and P03 were nearly 1 DN per year, which after seven years accumulated to an offset between PO1 and P03 of 0.68 bar, or more than 7 DN. It is needless to say that these drift rates are severe enough to have impacts on the maneuver performance analysis and propellant consumption calculations.

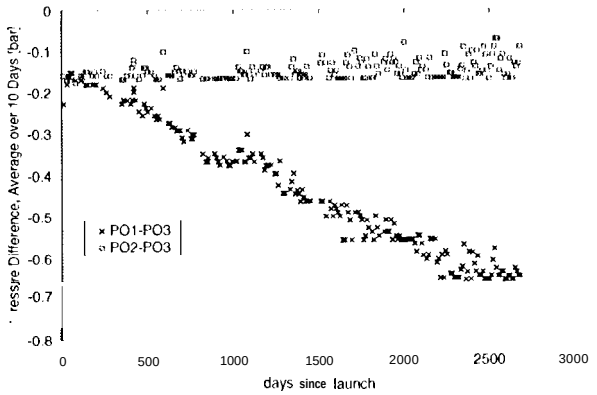

Figure 31: NTO Pressure Transducer Drifts

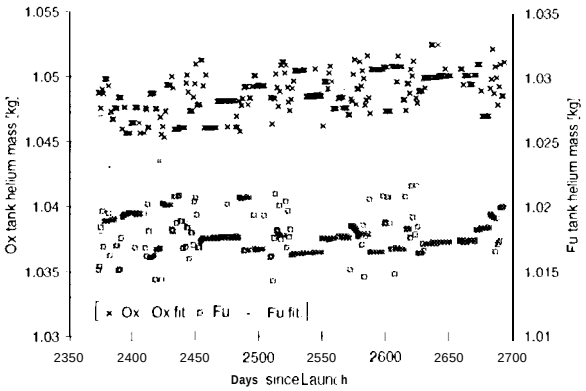

Figure 32: Helium in Propellant Tanks Post-PJR Without Drift Correction

It was not possible to determine the absolute drift rates of the pressure transducers until a pyro valve was fired to cut off the helium supply into the propellant tanks in March, 1996. Since then the propellant tank components have been isolated from each other via check valves in the pressurization lines. By using the thermodynamic relations between pressure, temperature and propellant content, the helium gas mass was calculated for the propellant tanks.

Figure 32 shows the results if the pressures were taken from the average of the three transducer readings respectively. The helium content of the MMH tanks appears constant within uncertainties. However, on the NTO side a considerable upward drift is visible. Besides the transducer drift, an overestimation of the propellant consumption would also cause an apparent upward drift in the helium content. However, even a 3σ uncertainty in propellant consumption cannot account for the observed slope. There was no temperature trend over this time period. And an increase in helium mass in the NTO tanks while at higher pressure than in the MMH tanks seems physically impossible.

The simplest explanation for this behavior is a corresponding upward drift of the NTO tank pressure reading. Indeed, the assumption that PO1 is drift-free and P02 and P03 are drifting at nearly the same rate resolves this issue. Figure 33 shows that the helium in the NTO tanks stays constant in such a case. It is now believed that in the true drift scenario P02 and P03 are drifting at nearly the same rate (0.078 bar/year), while PO1 is essentially not drifting.

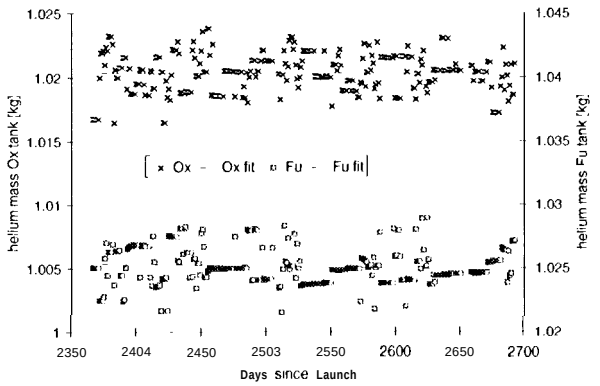

Figure 33: Helium in Propellant Tanks Post-PJR With Drift Correction

A more advanced method was necessary to evaluate the helium pressure transducer drift rate due to the larger quantization steps of 1.08 bar/DN. Right at the toggle point, the pressure is known most accurately; i.e., the average of the two values. By calculating the helium mass only at those toggle points, the much better resolution of the temperature sensors determines the data spread. During intervals without helium flow, a drift in the calculated helium mass is directly related to a pressure transducer drift. Two time periods of comparable size were chosen to determine the apparent pressure transducer drift rates at two different pressure levels. Before pressure regulator isolation there was only one period large enough without helium flow (see also chapter XII, Figure 36) between October, 1993, and September, 1994 (pre-ODM). The other period comprises the time after pressure regulator isolation March, 1996, until April, 1997 (post PJR).

From Figure 34 and Figure 35 an upward slope in the Helium mass is apparent in both

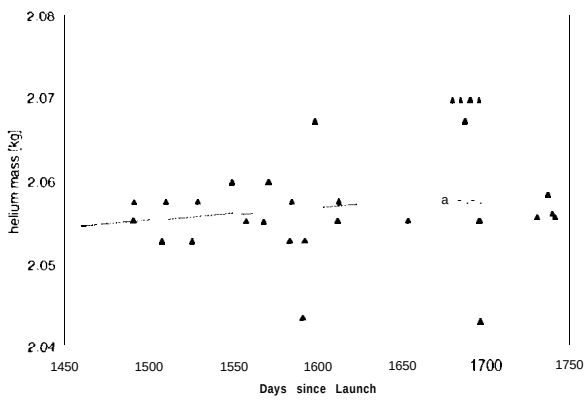

Figure 34: Helium Tank Contents Pre-ODM

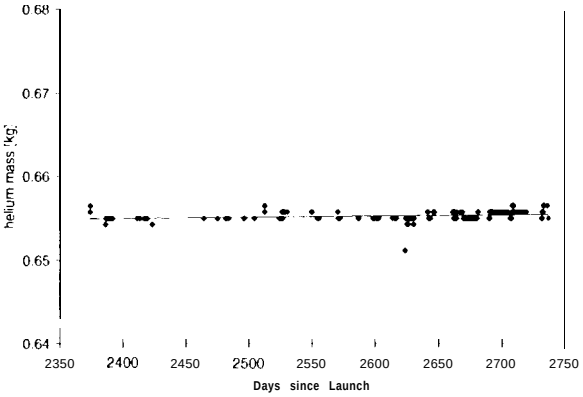

Figure 35: Helium Tank Contents Post-PJR

cases. The derived linear drift rates are 0.40 ±0.13(1σ) bar/year pre-ODM (Figure 34) and 0.039 ±0.001(1σ) bar/year post-PJR (Figure 35). The more recent data suggest that the helium pressure transducer is very stable with respect to drifting at the current pressure of 44 bar. However, earlier in the mission the drift rate could have been ten times—with a high uncertainty-as large at a pressure above 140 bar. There is not sufficient data to decide whether this effect is time related or dependent on the absolute pressure level.

This investigation shows that the total measurement error of two of the pressure transducers (P02 and P03) exceeded the requirement of ±2% full scale after 6.2 years in orbit. It should be stated, though, that the specified in-orbit operating life (6 years) has been surpassed and the specified ground shelf life (5 years) was already exceeded at launch—the sensors were shipped 1980.

X11. **Helium Budaet**

The RPM Analysis Team tracks the total helium mass on the spacecraft as a function of time. This total should remain nearly constant, since only 48 g of helium out of approximately 2700 g loaded is dissolved in the liquid propellants and expelled along with them during maneuvers. Helium should just relocate from the pressurant tanks to the propellant tanks during periods of pressure regulation. Therefore, since the amount of ullage helium in each tank is calculable from spacecraft telemetry assuming a certain propellant mass in the tanks, the total may be added up to verify that it is invariant. This so-called “helium budget” offers an independent check of the health of the propulsion system (particularly with regard

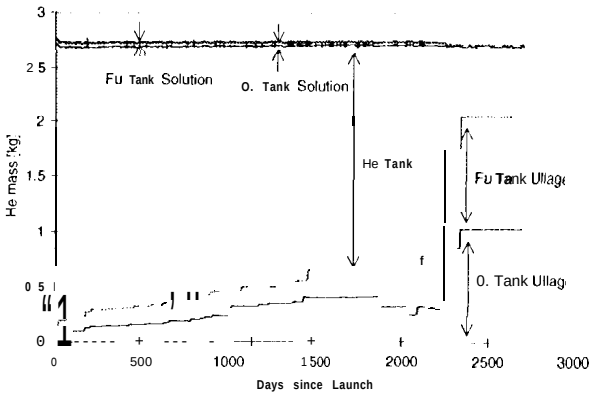

Figure 36: RPM Helium Budget

to possible helium or propellant leakages). Figure 36 represents a typical plot of the helium budget. The two curves at the bottom represent the helium in the propellant tanks; the top curve is the total helium.

Figure 37 is an enlarged view of the gaseous helium mass in the propellant and helium tanks. Although the curve in Figure 37 should have remained constant, it actually appears to increase until about day 1750. This apparent increase may be explained by a systematic error in the IO-N propellant consumption model used by the RPM Analysis Team of about 3%. This is very unlikely given the observed overperformance of the 10-N thrusters. However, a helium pressure transducer drift up to 0.4 bar/year might have occurred during the first five years, when the helium tank pressure was above 140 bar. A non-linearity in the helium pressure transducer calibration curve could also create this signature since the helium pressure decreased with propellant consumption. So far, there is evidence (see chapter XI) for making a pressure transducer drift in the high pressure range the most likely explanation.

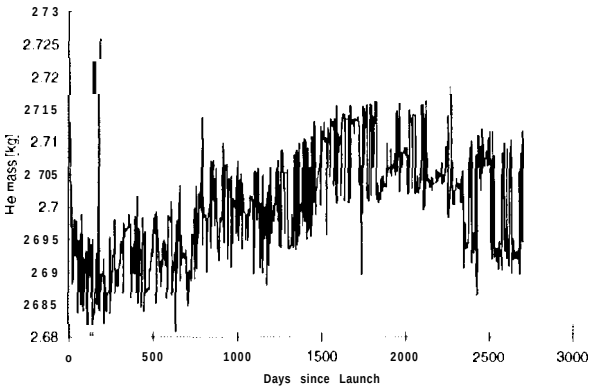

Figure 37: Total Gaseous Helium Mass

The three main 400-N maneuvers occurred at days 2110 (ODM), 2243 (JOI) and 2341 (PJR). The helium budget across ODM and JOI, which together consumed 44% of the total propellant loaded, seems to be flat. Figure 37 shows that it drops to a lower value at PJR, however. An error (near 3σ) in the propellant consumption at PJR could have caused this shift. Again, more likely is a non-ideal behavior of the helium pressure transducer during the drop from 63 bar to 44 bar across PJR.

The helium budget shows no evidence of an external or internal leak in the Galileo pressurization system. This demonstrates the utility of the Galileo teflon soft seat check valve and regulator design

XIII. Conclusions

The Galileo Retro-Propulsion Module has performed excellently throughout over seven years of flight operations, and Galileo navigation has been superb. The EOM propellant margin, defined at the ninetieth percent confidence level for ten satellite encounters in the Jovian system, has improved from -58 kg at launch to +49 kg. The RPM met the great challenges of interplanetary trajectory correction and attitude control during the six-year circuitous trip to Jupiter. Additionally, the 400-N engine successfully provided critical trajectory corrections three times during the mission, most notably at Jupiter Orbit Insertion, December 7, 1995 (PST).

Very few in-flight anomalies have occurred in the RPM through March, 1997. A total of four of the twelve 10-N thruster temperature transducers has failed open circuit, all within the first three years of the mission. This has had no operational impact on the RPM Team, since cluster temperature measurements adequately characterize 10-N thruster behavior. Some unexplained shifts in lateral thruster performance have been observed. However, maneuver delivery accuracy has still been excellent overall. In addition, some pressure transducers continued drifting linearly versus time, exacerbating attempts to analyze RPM performance.

Most notably, the Galileo NTO and MMH soft-seat check valves exhibited very high flowing ΔP's versus ground test levels. This effect, only

discernible during the three 400-N engine firings, had major programmatic implications for the Galileo project, particularly with respect to concerns of NTO vapor transport to the MMH lines and tanks. Specifically, flight power margins were maintained within tight limits, "on-the-shelf" 400-N maneuver sequences were extensively modified, and additional ground testing of NTO-contaminated check valves was undertaken.

The pressure regulator demonstrated exemplary performance during more than six years of operation, before finally being pyro-isolated following PJR. A calculated helium mass budget for the RPM demonstrated that there were no discernible internal or external helium leaks. Additionally, the helium mass budget also allowed a cross-check of propellant consumption, as well as characterization of the pressure transducer drift rates.

1O-N thruster performance has generally been 1 % to 5% higher than the best estimate for the ground-tested thrust levels. Many 10-N maneuver types were analyzed—all propulsive maneuvers (TCMs/OTMs) as well as spacecraft attitude turns and spin rate change maneuvers, in addition to some thruster flushing maneuvers.

400-N engine performance was excellent, particularly for JOI and PJR, due to very precise calibration of the Galileo accelerometers following ODM. Actual 400-N burn times were within 2-3% of ground predictions, which is quite good considering the deleterious effect of impeded check valve helium flow.

RPM consumables have been well within specifications. The prospects for completion of the Galileo nominal mission (as well as the Galileo Europa Mission) remain excellent. Operation of the Galileo RPM was a very challenging, highly rewarding experience for all personnel involved. The Galileo RPM experience offers a noteworthy model for success in international cooperation in spacecraft propulsion.

Acknowledgment%

The research described in this paper was carried out by the Jet Propulsion Laboratory, California Institute of Technology and the German Space Operations Center (GSOC), Division of the German Aerospace Research Establishment, DLR, under contracts with the National Aeronautics and Space Administration (NASA) and the Federal Republic of Germany (FRG) Bundesminister fur Forschung und Technologies (BMFT), respectively. The authors wish to acknowledge the following individuals who contributed to this research: N. Ausman, R. Barry, K. Bohnhoff, R. Cowley, K. Dar, B. Gounley, C. Guernsey, W. Hagenest, C. Jennings, R. Killinger, M. Landano, H. Long, K. Mantha, D. McPherson, T. Neilson, W. O'Neil, H. Schweig, W. Tyler, S. Tyler, J. Weiss.

References

' D'Amario, Louis A.; Bright, Larry E.; Byrnes, Dennis V.; Johannesen, Jennie R.; and Ludwinski, Jan M,: "Galileo 1989 VEEGA Mission Description," AAS Paper 89-431, August, 1989.

[2]Diaz, Al; and Casani, John R,: "Galileo on Track to Jupiter," Astronautics & Aeronautics, February, 1983.

[3]Jones, C. P.; and Landano, M. R.: "The Galileo Spacecraft System Design," AIAA Paper 83-0097, January, 1983,

[4]Bohnhoff, K., "Retro Propulsion Module (RPM) Bipropellant Unified System for Galileo," IAF Paper 82-326, September, 1982,

' Immich, H.; Langel, G.; and Munding, G.: "Satellite Unified Bipropellant Propulsion System Experiences and Improvements," AIAA Paper 89-2506, July, 1989.

[6] Barber, T.J.; Krug, F.A. and Froidevaux, B. M.: "initial Galileo Propulsion System In-Flight Characterization" AIAA Paper 93-2117, June, 1993,

[7]Cole, T. W.; Frisbee, R. H.; and Yavrouian, A. H.: "Analysis of Flow Decay Potential on Galileo," AIAA Paper 87-2016, June, 1987.

[8] Gotzig, "Galileo Test Report for 1O-N Thruster S/N 16 Pulse Performance, Low Temperature Start-Up and Delta Life Tests," DASA Document RPM-TR 1500-91-16, July, 1992

[9]Kühne, J. F.W., "Galileo - RPM Updated 10-N Thruster Performance Model (Based on S/N 16- May 1991 Tests)," DASA Document RPM-PN 1500-92-01 A, October, 1992